Light beam propagation in complex crystals

PhD Thesis by: **Nikhil P. Kumar**

Article-based thesis

PHD THESIS

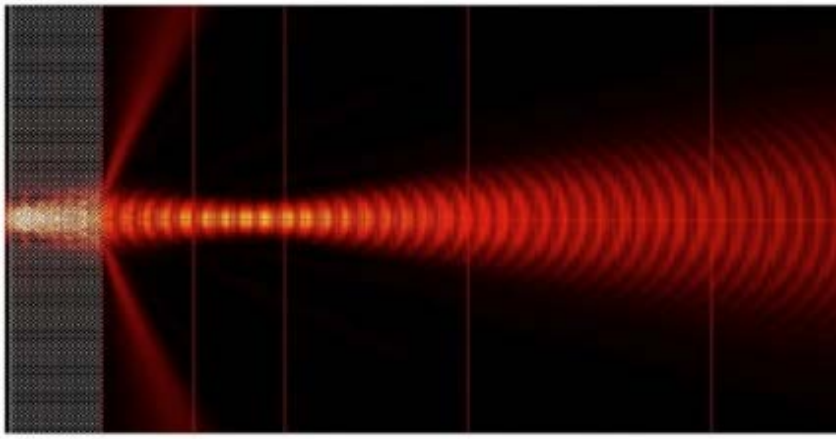

Supervised by:

Kestutis Staliunas

Muriel Botey

Ramon Herrero

Terrassa, July 2017

Politechnic Univeristy of Catalonia

Physics department

Index

Acknowledgments

Foremost, I would like to thank my advisors Kestutis Staliunas, Muriel Botey and Ramon Herrero for providing me an opportunity to complete my PhD thesis at Universitat Politechnica de Catalunya. I would like to thank Kestas for the guidance and support he gave during the entirety of my stay in Terrassa. Muriel and Ramon, for their immense patience and for essentially beating this thesis out of me.

I would like to thank Lina, Yu-Chieh and Shubham for the help and support they provided as colleagues and more over as friends. Ramon Vilaseca, Martha, Jordi Tiana, Jordi Zamora, Pau, Lorena and Cristi for the support during my initial days in DONLL.

Oscar, Sundar and Alejandro for making my stay in Terrassa as memorable as it has been.

Thanks to Princy, Geordie, Maya, Naru, Praveen, Subin, Patricia and Bhagya for bringing Kerala to Barcelona.

Ranjith, Vaibav, Javed are a few among the large contingent of Indian diaspora in Barcelona who brought back the flavour of home. Thanks for those dinners and conversations.

Avinash, Kattia, Nuno, Sruthi, Dani and the RESA group for the fun trips and memorable weekends.

I would like to thank Prof. Rangarajan, Dr. Ravindra, Prof. Dipankar , Dr. Nagaraju, Prabhu, Sharika and the entire NLST team for the support they

have given me at Indian Institute of Astrophysics. Sincere thanks to Prof Jagdev Singh for reminding me about the thesis after every one of those discussions.

My sincere gratitude to Mr. Sunil, Mr. Jijesh, Mr. Raison among many other high school teachers who helped me up here.

Apoorva, thanks for being the pillar rock.

and to my parents, Pradeep and Pushpa for being my north star.

List of publications

I M. Botey, R. Herrero, N. P. Kumar, R. Vilaseca, and K. Staliunas, *"Self-collimation and spatial filtering in 2D gain/loss periodic spatially modulated materials",* in European Quantum Electronics Conference (p. EI_P8) Optical Society of America (2011)

II N. P. Kumar, M. Botey, R. Herrero, and K. Staliunas *"High-directional wave propagation in periodic loss modulated materials"* Photonics and Nanostructures-Fundamentals and Applications **10**.4, 644-650 (2012)

III N. P. Kumar, M. Botey, R. Herrero and K. Staliunas, *"Flat lensing by periodic loss-modulated materials",* Journal of the Optical Siciety of America B **30** (10) 2684-2688 (2013)

IV M. Botey, N. P. Kumar, R. Herrero, L. Maigyte, R. Pico, and K. Staliunas, *"Negative diffraction by a periodically modulated loss",* Transparent Optical Networks (ICTON), 2013 15th International Conference on. IEEE, (2013)

V N. P. Kumar, L. Maigyte, M. Botey, R. Herrero, and K. Staliunas, *"Beam shaping in two-dimensional metallic photonic crystals",* Journal of the Optical Siciety of America B **31**(4), 686-690 (2014)

VI M. Botey, N. P. Kumar, L. Maigyte, R. Herrero, and K. Staliunas, *"Managing spatial diffraction through a periodic loss modulation"*, in SPIE Photonics Europe (pp. 912710-912710). International Society for Optics and Photonics (2014)

VII R. Herrero, M. Botey, N. Kumar, K. Staliunas, *"Dispersion management in spatially modulated broad band semiconductors",* 13th International Conference on Transparent Optical Networks. IEEE, (2011)

VIII R. Herrero, M. Botey, N. P. Kumar, and K. Staliunas, *"Spatial noise reduction in broad area semiconductors",* Transparent Optical Networks (ICTON), 2012 14th International Conference on Transparent Optical Networks. IEEE (2012)

IX R. Herrero, M. Botey, N. P. Kumar, and K. Staliunas, *"Improving beam quality in broad area semiconductor amplifiers",* SPIE Photonics Europe. International Society for Optics and Photonics,(2012)

X J. Tiana, J. Zamora, C. Nistor, V. Roppo, L. Maigyte, A. Aragoneses; N. Kumar, C. Martinez, J. Fernandez, C. Serrat, J.L. Font, R. Herrero, C. Cojocaru, J. Trull, C. Masoller, K. Staliunas, M.C. Torrent, J. Garcia, R. Vilaseca, "*Research activities of the group on nonlinear dynamics, nonlinear optics and lasers (DONLL) at the Universitat Politècnica de Catalunya" (Campus de Terrassa),* Óptica Pura y Aplicada **44**, (2011) (2011)

Chapter 1

Preface

The invention of laser half a century ago, brought about the emerging field of Photonics: the science of light. Recent advancement in Photonics have brought about a new era of miniaturisation of devices. Integrated optoelectronic devices of micro-meter scale play an important role in faster and safer means of Communication and information transfer. Along came a need for technology to allow the manipulation of light at the micrometer scale, with precise control over beam propagation. The past decades have been an intense research on novel photonic nanostructures, and new metamaterials to expand the possibilities to engineer the propagation of light

Since the pioneering works of E. Yablonovich and S. John [Yab87, Joh87] the number of scientific studies devoted to look for new structures, materials and specially functionalities has grown exponentially. From 1990 to 2010 there was initial intensive research in the field of periodic nanophotonic structures, the so-called Photonic Crystals (PhC), which lead to the discovery of amazing new features, from frequency band-gaps, to slow light, light localization in defects, applications for nonlinear phenomena, inhibition of spontaneous emission, wave guiding in planar structures or in PhC fibers. Moreover, all these peculiarities rapidly jump from being theoretical predictions to be experimentally demonstrated phenomena [Mart90, Bla00, Russ03, Noda03, Vla05, Dud06] or even to the discovery of their presence in nature [Vuk03].

Initially, PhC showed the ability to modify the dispersion relations in the frequency domain results therefore leading to temporal effects. The temporal dispersion is the relation between angular frequency ω and wave vector k, and it is modified due to the periodic modulation of refractive index, that is to say $\omega(k)$. However, it also affects the spatial dispersion. Thus, for a given frequency given ω, the relation between the spatial components of the wavevector, for instance k_x and k_y, is simultaneously modified. This modification in the spatial dispersion curve $k_x(k_y)$ affects diffraction, leading to different beam propagation effects such as, self-collimation [Hos99, Chi03, Sta06,], focalization and imaging behind the PhC structure [Luo02, Chub03, ,Ber04, Sav09], spatial (angular) filtering [Sta09, May10, Col10], and negative refraction [Cub03, Dec08] to even invisibility [Van08].

However, as it is evident from the well-known Kramers–Kronig relations [Luc05], that modulation of the refractive index is accompanied by a modulation of absorption or emission. Moreover, near resonance, the effects of absorption/emission can become relevant and have to be taken into account in addition to beam propagation effects arising from refractive index modulations. As a result, more recently, attention was paid to equally accessible artificial nanophotonic structures, where gain and losses are modulated on the wavelength scale: Gain Loss Modulated Materials (GLMMs).. The concept of GLMMs in one dimension (1D) was, in fact, previously considered in the context of distributed feedback lasers [Chen08], quantum well lasers and semiconductor arrays [Ult06].

The main differences of light propagation through gain/loss or index modulated media may be easily explained using the corresponding dispersion curves ω(k) (see the schematic representation of Fig. 1, just considering the case of two interacting modes). In the case of a one-dimensional index modulated media, eigenfrequencies remain real and only the phase velocity of the wave is modified by mode coupling. At resonance frequencies push appear and Photonic Band Gaps (PBG) appear; inhibiting light propagation since no wavevector is available at the PBG frequencies (see Fig. 1.1a). On the contrary, gain/loss modulated media affect both the real and imaginary parts of eigenfrequencies and thus, also the gain/absorption can be modified through the mode coupling. At resonance frequencies lock and complex modes develop being either amplified or decreasing depending on the complex component $\omega_{im}(k)$ (see Fig1.1b,c). The appearance of sharp peaks in $\omega_{im}(k)$ corresponds to an anisotropic gain in the k-space. This angular dependence on gain gives rise to spatial filtering effects as well.

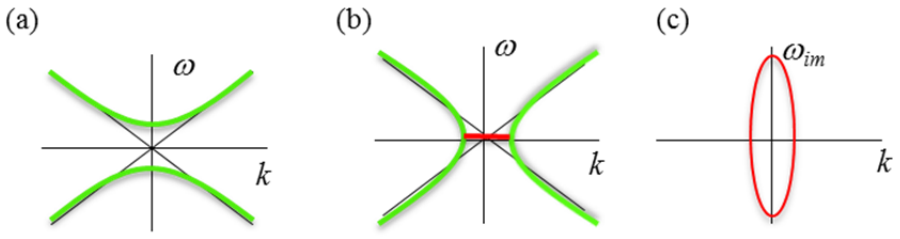

Fig. 1.1 Schematic dispersion curves of a PhC(a), GLMM(b) and the anisotropic gain in k-space present in GLMMs(c). The black lines denote ω(k) for an homogenous media

The idea to apply photonic nanostructures to engineer the spatial profile of light beams was first proposed just before I started my PhD research, and precisely developed in the group where I did my PhD. Self-collimation, super-diffusion and flat focalisation where predicted along with the presence of high directive gain [Sta09] [Bot 10]. Developing such ideas in specific systems, and binging them closer to applications has been the main objective of my PhD.

The work of my PhD was devoted to understand the beam propagation effects in GLMMs, identify the spatial propagation effects exhibited by such materials and propose realistic scenarios in which LMM can be implemented in existing and evolving technology and devices. We built our studies from a solid understanding of GLMMs published in prior studies [Sta09], which is however based on the paraxial approximation, which reduces the accuracy of the predictions by a large scale. Paraxial approximation excludes wavevectors of the beam which are propagating at a large angle.

The methodology adopted in our study is a combination of analytical prediction and numerical confirmation of the predicted effects. Analytical predictions combine the full plane wave expansion model and a truncated couple mode expansion of Maxwell equations. Concerning numeric beam propagation experiments, we used Finite Difference Time Domain (FDTD) method to numerical propagate the light beam through a periodically loss modulated media. FDTD computes the full set of Maxwell's equations and involves no approximation.

As predicted by the plane wave expansion method, the propagation of light beams within such structures is sensitive to the propagation direction. We provided a numerical proof in 2D periodic Loss Modulated Materials (LMM) with square and rhombic lattice symmetry, by solving the full set of Maxwell's equations, using the finite difference time domain method, which entails no approximation. Anisotropy of amplification/attenuation leads to the narrowing of the angular spectrum of beams with wavevectors close to the edges of the first Brillouin Zone. The effect provides a novel tool to filter out high spatial harmonics from noisy beams, while being amplified. A later study lead us to analyse the focalisation performance of a flat LMM slab. Flat lensing was analytically

predicted by the dispersion curves obtained from a coupled mode expansion of Maxwell's equations, and then numerically confirmed. For a range of frequencies coinciding with a high transmission window at resonant Bragg frequencies (bandgap frequencies for PhCs), light beams undergo negative (anomalous) diffraction through LMMs. The phase shifts accumulated within the structure are then compensated by normal diffraction in free space, leading to a substantial focalization beyond it. The predicted phenomena are generic for spatially modulated materials and other kinds of waves. Thus, we also discussed, for the first time, propagation in LMM acoustic crystals, predicting high angular transmission bands.

While these initial studies assumed hypothetical LMM materials, in a realistic scenario, loss modulations are always accompanied by refractive index modulations, as predicted by Kramers-Kronig relations. During the final phase of my PhD, we focused on more realistic structures exhibiting both index and loss modulations, namely metallic photonic crystals (MPhCs), made of 2D rhombic arrays of metallic cylinders embedded in air. We explored their ability to tailor the spatial propagation of light beams. Indeed, MPhCs support self-collimated propagation and negative diffraction. In this later case, flat lensing was demonstrated, leading to the focalization of beams behind MPhCs slabs. Also, the anisotropic attenuation of light within MPhCs enables spatial filtering.

Finally, we initiated studies towards the implementation of GLMMs. One of such possible applications are Broad Area Semiconductor (BAS) amplifiers, or ultimately BAS lasers. BAS (also referred as edge emitting lasers) are technologically relevant light sources which main advantage being their high conversion efficiency. Their planar configuration enables efficient access of the pump to the whole volume of the active amplifying medium. However, BAS lasers suffer from a serious disadvantage as the spatial quality of the emitted beam is relatively low [Bur99]. If no special mechanisms are incorporated in the design, the emission has a broad and noisy optical and angular spectrum. The poor spatial quality is principally due to the absence of a natural angular selection mechanism in the large aspect-ratio cavity of such devices. In absence of cavity mirrors such planar semiconductor structures can act as light amplifiers, BAS amplifiers. We realize preliminary studies to show that GLMMs may

act in BAS amplifiers as an intrinsic mechanism to improve the beam quality emission.

The original work performed during my PhD along these lines, resulted in three published papers [Kum12, Kum13, Kum14] (where I am always the first author) and six conference papers [Bot11, Bot13, Bot14, Her11, Her12, Herr12-2]. Therefore, in this way this PhD is based on the three published papers and six conference proceedings, being organized as follows.

Chapter 2 provides an overview the general properties of complex crystals methods used in the thesis.

In Chapter 3 we describe how LMM support beam spatial effects such as spatial filtering, flat lensing or self-collimation, through a new mechanism, different from the case of PhCs.

Chapter 4 is devoted to beam shaping in MPhCs, being modulated in the both real and imaginary components, however being only lossy, no gain is present. We show how this kind of complex structures also hold non-diffractive propagation and, negative diffraction leading to flat lensing and spatial filtering.

The application of the previous results being used to improve the beam quality of BBAS amplifiers is discussed in Chapter 5.

Finally, Chapter 6 summarizes the results and presents the conclusions of the thesis, as well as, a discussion on future perspectives.

Along the development of my PhD, we proposed, analyzed and established spatial beam propagation effects in GLMM, from purely ideal LMM structures to more realistic structure as MPhCs or BAS amplifiers.

Chapter 2

Introduction to Complex Crystals

Chapter index

2.1 Light waves propagation

The first nanostructured artificial materials studied to control the light propagation were made of dielectric materials. They were called Photonic Crystals (PhC) for their ability to affect the propagation of photons analogously to energy bands for electrons in solids.

Early in 1887 the English physicist Lord Rayleigh [Ray88] experimentally demonstrated the existence of photonic band-gaps (PBGs) as forbidden propagation bands for certain frequency ranges. Research interest grew with the publication of two milestone papers in 1987 by E. Yablonovitch [Yab87] and S. Johnwork [Joh97], who pointed out the potential applications of such structures in the control of spontaneous emission of materials embedded in them, or in the localization of light. [Sak04, Joa11, Sou12]

Periodic nanostructures with modulations on the wavelenght scales can be build one, two, or three dimensions being fabricated with a large variety of methods that include drilling holes, stacking layers, direct laser writing, or self-assembly of spheres. More recently the assembly of new materials such as metals or semiconductors has lead to the general concept of Complex Crystals which hold exotic properties not only involving waves, frequency PBG or guiding wavelengths but also affecting the propagation of light beams, finding applications wherever light must be manipulated.

2.1.1 Coupled mode: Two mode case and temporal dispersion

In order to model the propagation of light trough a periodic nanostructure, we start from the wave equation as directly obtained from the Maxwell equations, which in terms of the electric field reads:

$$\vec{\nabla}\times\vec{\nabla}\times\vec{E} = -\varepsilon(\vec{r})\frac{1}{c^2}\frac{\partial^2\vec{E}}{\partial t^2} \qquad \text{Eq.(2.1)}$$

Here $\varepsilon(\vec{r})$ is the relative electric susceptibility of the material, which in the most general approach may consists on a real part (corresponding to the refractive index) as well as an imaginary part (corresponding to

losses or gain). In general, the ratio between the real and imaginary parts of such susceptibility depends on the materials. As it is evident from the well-known Kramers–Kronig relations, a modulation of the refractive index can be accompanied by a modulation of absorption or emission. Moreover, near resonance, the effects of absorption/emission can become relevant and have to be taken into account in addition to beam propagation effects arising from refractive index modulations. As a result, beyond PhC the new problem to be considered is light propagation within materials that incorporate in phase index and gain/loss modulations. The concept of gain/loss modulation in 1D was considered previously in the context of distributed feedback lasers [Chen08], quantum well lasers and semiconductor arrays [Ult06].

This approach is mainly devoted to simple harmonic optical potentials which allows describing the field with a reduced number of modes. Consider the simplest case of a 1D material presenting a sinusoidal modulation in the permittivity $\varepsilon = 1 + 2im\cos(qz) = 1 + im(e^{iqz} + e^{-iqz})$ with amplitude *m* and a given wavenumber *q*. The propagation along the material of a linearly polarized monochromatic harmonic electric field with amplitude $E(z,t) = E(z)e^{-i\omega t}$ is simply determined by the form:

$$-\frac{\partial^2 E(z)}{\partial z^2} = \varepsilon(z)\frac{\omega^2}{c^2}E(z). \qquad \text{Eq.(2.2)}$$

The field can be written as the incident field and the corresponding harmonics introduced by the direct interaction with the modulated material in the form of a Plane Wave Expansion:

$$E(z) = e^{ikz}\sum_j a_j e^{i(qj)z}. \qquad \text{Eq.(2.3)}$$

Next, we analyze the interaction between two of these modes, e.g. modes with wavenumbers *k* and *k-q*. Introducing the field and material modulation in the propagation equation and grouping terms with the same exponential factor, one obtains the equations coupling these two modes:

$$\begin{aligned}(k^2-\frac{\omega^2}{c^2})a_0-im\frac{\omega^2}{c^2}a_1=0\\((k-q)^2-\frac{\omega^2}{c^2})a_1-im\frac{\omega^2}{c^2}a_0=0\end{aligned} \quad \text{Eq.(2.4)}$$

Shifting the (k,ω) origin to the crossing point $(k_0,\omega_0),k_0=\frac{q}{2},\omega_0=ck_0=\frac{cq}{2}$, where *c* corresponds to the light velocity inside the material, the new equations becomes symmetric:

$$\begin{aligned}\left[\left(k+\frac{q}{2}\right)^2-\left(\frac{\omega}{c}+\frac{q}{2}\right)^2\right]a_0-im\left(\frac{\omega}{c}+\frac{q}{2}\right)^2a_1=0\\\left[\left(k-\frac{q}{2}\right)^2-\left(\frac{\omega}{c}+\frac{q}{2}\right)^2\right]a_1-im\left(\frac{\omega}{c}+\frac{q}{2}\right)^2a_0=0\end{aligned} \quad \text{Eq.(2.5)}$$

Near the crossing point (k_0,ω_0) the equation set has the simple analytical form:

$$\begin{aligned}\left[\Delta k-\frac{\Delta\omega}{c}\right]a_0-im\frac{k_0}{2}a_1=0\\-\left[\Delta k-\frac{\Delta\omega}{c}\right]a_1-im\frac{k_0}{2}a_0=0\end{aligned} \quad \text{Eq.(2.6)}$$

where $\Delta k=k-k_0$ and $\Delta\omega=\omega-\omega_0$ are the deviations from the degeneracy point. The analytical relationship between the frequency and the wavenumber deviations is the simple form:

$$\Delta\omega=\pm c\sqrt{\Delta k^2-\frac{m^2k_0^2}{4}} \quad \text{Eq.(2.7)}$$

This problem can be faced as a wave with a real wavevector evolving in time within the structured material (an initial condition problem, $\Delta\omega(\Delta k)$) or as a wave with a defined real frequency propagating along the complex crystal (a boundary condition problem, $\Delta k(\Delta\omega)$). In the first, modes have a complex valued frequency ω being the real part of ω the wave frequency and its imaginary part the temporal grow/decay exponent. In the second, waves with real frequency ω propagate through the medium with a complex *k* wavenumber, being its imaginary part the spatial grow/decay exponent. Here, we consider real wavenumbers to obtain complex eigenfrequencies.

Considering real values of the modulation amplitude in permitivity $m = m_r + im_i$, $m_i = 0$, i.e. the Photonic Cristal (PhC) case, eigenvalues given by the "initial value problem" $\Delta\omega(\Delta k)$ are real, as shown in Fig. 2.1.

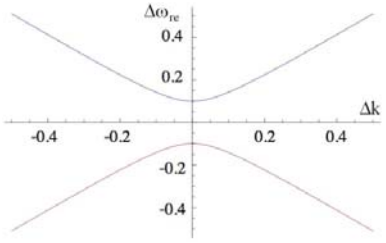

Fig. 2.1 Dispersion relation. Frequency ω (in normalized units $c\pi/a$ where a is the lattice constant) versus wavenumber k (in normalized π/a units).

In general, for a complex value of the coupling, the matrix is not hermitian, and the eigenvalues of the problem are not necessarily real-valued. The real parts of the eigenfrequencies, as in the case of PhCs, correspond to the frequencies of the Bloch modes and the imaginary part of the frequency is the net gain or loss of the corresponding Bloch mode. For the case of purely imaginary modulations, that is to say for a modulation amplitude in permitivity $m = m_r + im_i$, $m_r = 0$, eigenvalues become complex-conjugated near resonance and real and imaginary parts are represented in Fig. 2.2.

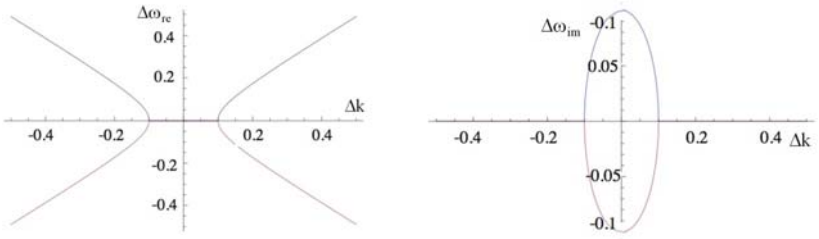

Fig. 2.2 Real (left) and imaginary (right) part of the dispersion relation. Frequency ω (in normalized units $c\pi/a$ where a is the lattice constant) versus wavenumber k (in normalized π/a units).

For the purely imaginary the dispersion curves of the uncoupled modes (dashed curves) do not “push” mutually as it is in the case of PhCs to form the bandgap around their cross point, but rather pull one-another and lock to some common frequency. The width of the locking area is $m_0 q / 2$ as follows from eq. 2.7.

2.1.2 Plane Wave Model in Photonic Crystals

The Plane Wave expansion Method (PWM) is a well-established modal method to solve the wave equation as an eigenvalue problem, based on the Floquet-Bloch theorem for periodic systems, see for instance [Ho90] [Joh01]. Analogously to the coupled mode expansion, we shall start by the wave equation in a non-permeable space ($\mu=\mu_0$), instead of eq. 2.1, it is here more convenient to consider the magnetic field $\vec{H}(r,t)$. Assuming harmonic plane waves $\vec{H}(r,t) = H(r)e^{i\omega t}$, the Helmholz's equation:

$$\nabla \times \frac{1}{\varepsilon(\vec{r})} \nabla \times \vec{H}(\vec{r}) = \frac{\omega^2}{c^2} \vec{H}(\vec{r}) \qquad \text{Eq.(2.8)}$$

where $\varepsilon(\vec{r})$ is any periodic function in space, $\varepsilon(\vec{r}) = \varepsilon\left(\vec{r} + \vec{R}\right)$ with $\vec{R} = n_1\vec{a}_1 + n_2\vec{a}_2 + n_3\vec{a}_3$ being $\{\vec{a}_1, \vec{a}_2, \vec{a}_3\}$ the primitive direct lattice vectors of the periodicity. According to the Floquet-Bloch theorem the solutions to Eq. 2.8 can be chosen in the form of periodic functions of the wavevector $\vec{k}$ meaning that the solution at $\vec{k}$ is the same that the solution at $\vec{k} + \vec{G}$, being $\vec{G}$ a reciprocal lattice vector which may be expressed as $\vec{G} = m_1\vec{b}_1 + m_2\vec{b}_2 + m_3\vec{b}_3$ being $\{\vec{b}_1, \vec{b}_2, \vec{b}_3\}$ the reciprocal lattice vectors defined as $\vec{a_i} \cdot \vec{b_j} = 2\pi\delta_{ij}$.
In turn, $\varepsilon(\vec{r})$ can be expanded into a Fourier series of all reciprocal vectors, $\vec{G}$:

$$\varepsilon(\vec{r}) = \sum_{\vec{G}} \varepsilon(G) e^{i\vec{G}\vec{r}} \quad \vec{H}(r) = \sum_{\vec{G},p} h_{G,p}\hat{e}_p e^{i(\vec{k}+\vec{G})\vec{r}} \qquad \text{Eq.(2.9)}$$

Where *p=1,2* stands for the two polarizations, perpendicular to the propagation direction $\vec{k} + \vec{G}$. Then, using the expansion of Eq. 2.9 may be rewritten for 2D systems decoupling modes for both polarizations, TM and TE, as:

$$TM: \qquad \sum_{G'} \left|\vec{k} + \vec{G}\right|\left|\vec{k} + \vec{G}'\right| \varepsilon^{-1}_{G-G'} \cdot H_{1,G} = \frac{\omega^2}{c^2} H_{1,G'} \qquad \text{Eq.(2.10a)}$$

$$TE: \qquad \sum_{G'} \left(\vec{k} + \vec{G}\right) \cdot \left(\vec{k} + \vec{G}'\right) \varepsilon^{-1}_{G-G'} H_{2,G} = \frac{\omega^2}{c^2} H_{2,G'} \qquad \text{Eq.(2.10b)}$$

This leads to an Hermitian eigenproblem over the primitive cell of the lattice at each Bloch wavevector *k*. This primitive cell is a finite domain if the structure is periodic in all directions, leading to

discrete eigenvalues labelled by n= 1,2,.... These eigenvalues $\omega_n(k)$ are continuous functions of k, forming discrete *bands* when plotted with respect to k, in a *band diagram* or *band structure*. Such temporal dispersion relations map all possible plane waves in the system. Besides, the solutions are periodic in k, meaning that the solution at k is equal to the solution at $k+G_j$. . Thanks to this periodicity, it is sufficient to compute the eigensolutions for k within the primitive cell of this reciprocal space or First Brillouin Zone (FBZ). This folding of the dispersion relations is shown in the Band Diagram of a 1-dimensional (1D) structure with $R_1=a$ and $G_1=2\pi/a$, then the FBZ would correspond to $k \in [-\pi/a, \pi/a]$, but due to the time-reversal symmetry the interval ($-k \leftrightarrow k$), it is reduced to $k \in [0, \pi/a]$. The shaded areas on Fig. 2.5 indicate the forbidden propagation bands or Photonic Bandgaps (PBG). The shaded areas indicate the forbidden propagation bands or PBGs.

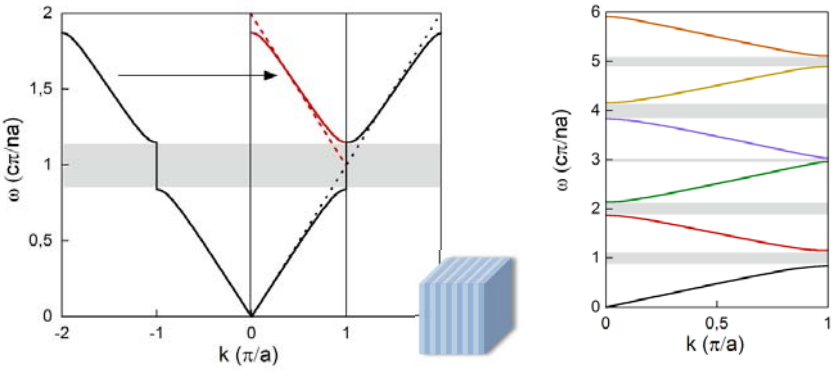

Fig. 2.5 Temporal dispersion relations (band structure) of a periodic 1D dielectric structure, as shown in the inset. Left: Frequency ω (in normalized units $c\pi/na$ where a is the lattice constant) versus wavenumber k (in normalized π/a units). The dotted lines represent the dispersion of a uniform 1D medium, and the vertical line determines the FBZ. The red curve represents the folded dispersion of the periodic medium. Right: Band diagram of the FBZ. The shaded domains indicate the PBG.

Note also that k is not required to be real; complex $k=k_{Re}+ i\ k_{Im}$ represent evanescent modes that can exponentially decay from the boundaries of a finite crystal, but which cannot exist in the bulk.

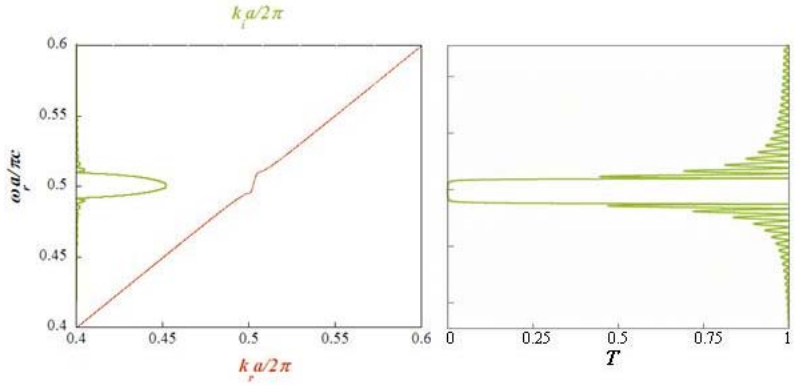

Fig. 2.6 Left: Complex wavevector. Right: Transmission. Both plotted with respect to the normalized frequency on the vertical axis.

Figure 2.6 shows the calculated valued for the real and imaginary components as well as the transmission from a finite 1D structure as the one in Fig. 2.5.

While during many years efforts were dedicated to find 3D photonic structures exhibiting a full PBG to completely inhibit the propagation of light (for all directions), most applications are based on 2D PhC. Such 2D structures are easily achievable to fabricate with the actual nanophotonic techniques and already hold the most important characteristics of PhC. One of the basic geometries used in 2D photonic crystals are cylinders embedded in air (or cylindrical holes embedded in a material) in a triangular, hexagonal or general rhombic geometry. For this configuration the TE/TM polarizations behave differently, being PBG bigger for TM (E parallel to the rods) in the case of rods. Figure 2.7 shows the Band diagram.

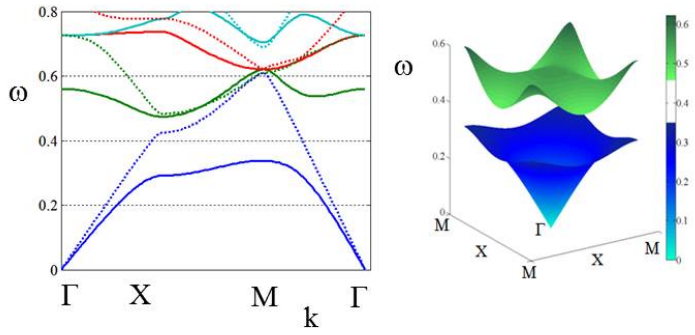

Fig. 2.7 Dispersion relation (band structure) of a periodic 2D square lattice made of rods in air dielectric PhC formed by rods in air. Left: Frequency ω (in normalized units $c\pi/na$ where a is the lattice constant) versus wavenumber k (in normalized π/a units). The dotted lines represent the dispersion of a uniform 1D medium, where the vertical line determines the shows the "folding" effect of applying Bloch's theorem with an artificial periodicity a, ω. The red curve represents the folded dispersion of the periodical medium. Right: Band diagram of the FBZ. The shaded domains indicate the PBG.

The PWE model may be regarded as an initial condition problem in the sense that the frequency of each spatial mode is determined for each given real-valued *k*, therefore this modal method is in principle useful to describe real periodic structures, that is to say, purely real-valued in PhCs where frequency is purely real-valued. However, for gain/loss modulated materials the imaginary part can be nonzero. Precisely such imaginary part determines the non-stationary growth

or decay of modes of ref. [Bot10], where the Plane Wave Expansion model is extended to be applied in systems where the gain and losses are modulated instead of the refractive index. This model is used in my PhD to obtain the band diagrams for both 1-D and 2-D GLMMs. The model underlines the existence of frequency locked modes instead of the opening of PBGs. It also re-iterated the existence of spatial beam propagation effects mentioned in the previous study.

2.2 Beam propagation in Complex Crystals

We consider the propagation of a monochromatic wave $\mathrm{E} = Ee^{-i\omega t}$ along a material structured in both, the transverse and longitudinal directions. The wave equation for the monochromatic wave is $\frac{\partial^2 \mathrm{E}}{\partial t^2} - \frac{c^2}{n^2}\nabla^2 \mathrm{E} = 0$ simplified for stationary fields $\frac{\partial E}{\partial t} = 0$ to the Helmholtz equation:

$$\nabla^2 E + \left(\frac{n\omega}{c}\right)^2 E = 0 \qquad \text{Eq. (2.11)}$$

Introducing the field amplitude A, the electric field of a plane wave can be written as $E = Ae^{i\vec{k}\vec{r}}$ and the propagation equation for the field amplitude can be written as

$$\nabla^2 A + 2i\vec{k}\vec{\nabla}A + (n^2 - 1)k^2 A = 0 \qquad \text{Eq. (2.12)}$$

where the wavevector $\vec{k} = (k_x, k_z)$ gives the propagation direction of the plane wave and its modulus is the wavenumber inside the material.

The studied beams propagate along structured materials in the x-z plane. The planar studied medium is sinusoidally modulated in refractive index and gain. The considered 2D sinusoidal modulation $n(x,z) = n_h + 2\Delta n\left(\cos(\vec{q}_1\vec{r}) + \cos(\vec{q}_2\vec{r})\right)$ has a homogeneous complex refractive index n_h and the modulated part with a complex amplitude Δn and geometry given by the two vectors $\vec{q}_1 = (q_x, q_z), \vec{q}_2 = (-q_x, q_z)$ where $q_x = q\sin\theta, q_z = q\cos\theta$ correspond to the transverse and

longitudinal modulation wavenumbers respectively and being 2θ the angle between the two generating vectors. The complex refractive index can be written as a product of transverse modulation and longitudinal modulation or alternatively in the exponential form:

$$n(x,z) = n_h + \Delta n\left(e^{i(q_x x+q_z z)} + e^{i(-q_x x+q_z z)} + e^{i(q_x x-q_z z)} + e^{i(-q_x x-q_z z)}\right) \quad \text{Eq. (2.13)}$$

The propagating light beams along the structured material can be now expanded as an addition of harmonics of the potential periodicities in the form $E(x,z) = \sum_{l,p} A_{l,p} e^{i\vec{k}_{l,p}\vec{r}} + c.c.$ where $\vec{k}_{l,p} = \vec{k} + l\vec{q}_1 + p\vec{q}_2$ and $A_{l,p}$ is the amplitude of each mode. The wave equation takes the expression:

$$\sum_{l,p}\left[\nabla^2 A_{l,p} + 2i\vec{k}_{l,p}\cdot\vec{\nabla}A_{l,p} - k_{l,p}^2 A_{l,p} + n^2 k_0^2 A_{l,p}\right]e^{i\vec{k}_{l,p}\vec{r}} = 0 \quad \text{Eq. (2.14)}$$

where $k_0 = \dfrac{2\pi}{\lambda}$ is the wavenumber in vacuum.

The introduction of the expanded field and potential $n(x,z)$ in the propagation equation results in a coupled system for the amplitudes of the harmonics. The modulation couples the neighboring modes, obtaining an equation for each one.

2.2.1 Coupled mode equations. Three mode case

In many cases, we are interested in the evolution of the beam envelope propagating in a given direction *z*. Its propagation is only related with the dispersion relation curves at small transverse wavenumbers that can be generally calculated just considering three harmonics, *(l,p)=(0,0),(0,-1)* and *(-1,0)*, the ones that intersect at the edge of the first Brillouin zone at resonance. The square symmetry is an special case for which not three but four modes intersect at resonance *(l,p)=(0,0),(0,-1) ,(-1,0)* and *(-1,-1)*.

Only considering these three principal modes, the system eigenvalues can be easily calculated from eq. 2.14. The complex index modulation amplitude determines the character of the mode coupling and creates bandgaps for PhC-like materials with real refractive index modulations or locking areas for gain/loss modulations as explained in Section 2.1.1. In the case of beam propagation this corresponds to angular bandgaps and gain propagation directions with amplifying and depleting modes (see Figure 2.8).

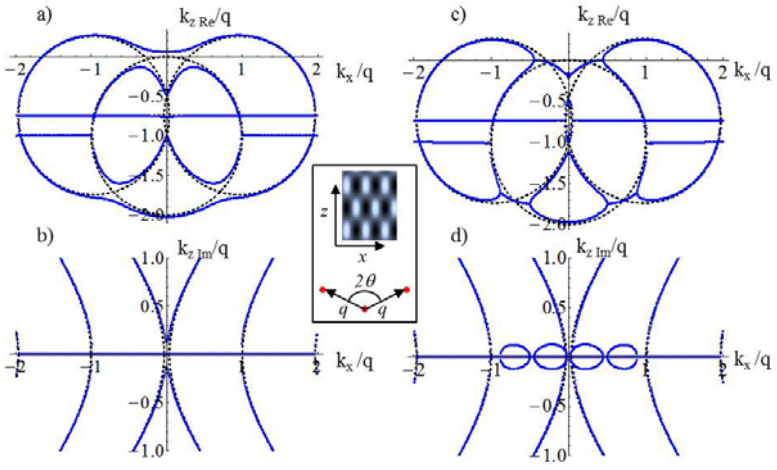

Fig. 2.8 Real and imaginary part of the eigenvalues for the three-mode model. a) and b) correspond to a photonic crystal like structure with m=0.1, q=75º and appearing angular bandgaps. c) and d) correspond to m=i0.1, q=75º appearing locking areas where eigenvalues become complex-conjugated.

2.2.2 Dispersion curvature and diffraction

Diffractive broadening of light beams is a fundamental phenomenon which geometrical interpretation is a different acquired phase shifts on the transverse modes composing the beam, i.e. the acquired phase depends on the propagation angle. This dephasing of the plane wave components results in a diffractive broadening of the light beam.

In general the positive (negative) diffraction means that the surfaces of constant frequency are concave (convex) in the wave-vector domain (see Fig. 29).

The continuous change from positive to negative curvatures on the surfaces of constant frequency assure the occurrence of the zero diffraction or self-collimation, supposed to occur in a particular point in the wave-vector domain where the curvature of the surfaces of constant frequency becomes exactly zero (Fig. 29 a). Self-collimation physically means that light beams of arbitrary width can propagate without diffractive broadening (Fig. 29 b).

The dispersion curvature can be modified by modulations of the refractive index and adjusting the parameters it is possible to obtain positive, negative and also nondiffractive regimes. For instance, eigenmodes with larger real eigenvalue in Figure 2.8 a presents a near zero curvature.

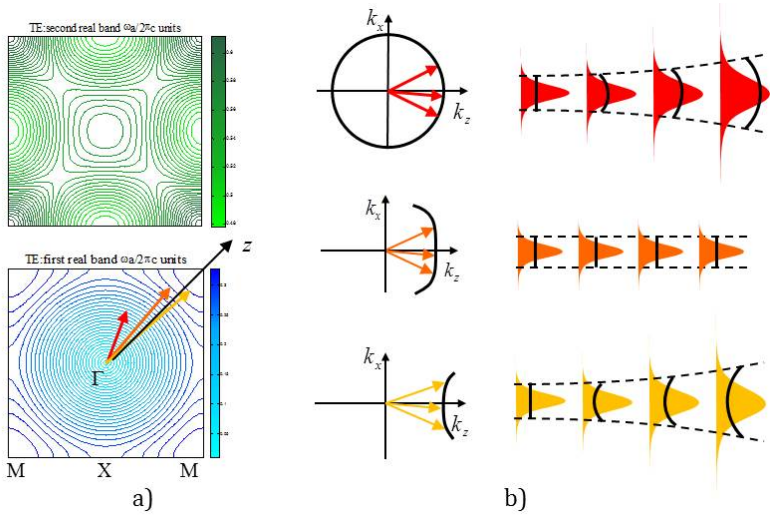

Fig. 2.9 a) Real isofrequency contours of the dispersion relation of Fig. 2.7. Down(up) contours correspond to the TE first (second) band. In z direction appear for an increasing frequency value a positive curvature (normal diffraction), flatness (non-diffraction) and negative curvature (negative diffraction). b) Representative schemes of beam shape evolution and accumulated phase (solid black line) for the three cases.

2.3 Numerical Methods in Complex Crystals

2.4.1 Paraxial Approximation

Assuming that the spatial period of the structure is significantly larger than the wavelength, the Slowly Varying Envelope

Aproximation can be applied and the propagation along the crystal can be well described by the paraxial approximation:

$$\frac{\partial A}{\partial z} = \frac{i}{2k}\frac{\partial^2 A}{\partial x^2} + i\frac{k}{2}(n^2 - 1)A \qquad \text{Eq.(2.15)}$$

where second derivatives in the propagation direction have been neglected. For small enough amplitudes of the spatial modulations of the refractive index Δn, the equation can be expressed as

$$\frac{\partial A}{\partial z} = \frac{i}{2k}\frac{\partial^2 A}{\partial x^2} + ik\Delta nA \qquad \text{Eq.(2.15)}$$

The periodic modulation of the complex refractive index allows the field expansion as an addition of harmonics as explained in Section 2, and the solvability of this linear system of equations results in the transverse dispersion relation of the studied material $k_z(k_x)$. We fix real values for the transverse wavenumber k_x to obtain complex eigenvalues k_z and the corresponding eigenfunctions of the system.

A sinusoidal modulation of the complex refractive index (Eq. 2.13) just couples the first neighboring harmonics and the field expansion can be truncated to five harmonics, $A(x,z) = e^{i\vec{k}\vec{r}}\left(A_{0,0} + A_{1,0}e^{i\vec{q}_1\vec{r}} + A_{-1,0}e^{-i\vec{q}_1\vec{r}} + A_{0,1}e^{i\vec{q}_2\vec{r}} + A_{0,-1}e^{-i\vec{q}_2\vec{r}}\right)$ with the corresponding equations

$$\left.\begin{aligned}
ik_z A_{0,0} &= -\frac{i}{2k}k_x^2 A_{0,0} + ik\Delta n\left(A_{1,0} + A_{-1,0} + A_{0,1} + A_{0,-1}\right)\\
i(k_z + q_z)A_{1,0} &= -\frac{i}{2k}(k_x + q_x)^2 A_{1,0} + ik\Delta nA_{0,0}\\
i(k_z - q_z)A_{-1,0} &= -\frac{i}{2k}(k_x - q_x)^2 A_{-1,0} + ik\Delta nA_{0,0}\\
i(k_z + q_z)A_{0,1} &= -\frac{i}{2k}(k_x - q_x)^2 A_{0,1} + ik\Delta nA_{0,0}\\
i(k_z - q_z)A_{0,-1} &= -\frac{i}{2k}(k_x + q_x)^2 A_{0,-1} + ik\Delta nA_{0,0}
\end{aligned}\right\}$$

The corresponding matrix will give the eigenvalues and eigenvectors of the linear system. The system can be even reduced to only three modes as explained in Section 2.2.1.

The paraxial equation can be numerically integrated by semi-spectral methods following a split-step method, i.e. by splitting every

time step into a first perfect integration of the diffractive term in Fourier space followed by a second Eulerian integration of the refractive index term in real space.

2.4.2 Finite Difference Time Domain method

The finite-difference time-domain (FDTD) method the most popular method used in computational electrodynamics [Cou28, Yee66, Taf80, Taf00]. It is the most important tool used for diffractive optics simulations. The ability to model light propagation, scattering, diffraction, reflecting and polarization effects are a unique combination of features of FDTD. It allows accurate and powerful computation of structures on wavelength scale with very fine structural details. High light confinement, which in turn corresponds to large refractive index of the medium, makes it suitable for simulation of semiconductor devices. We have extensively used FDTD in two spatial and one temporal dimensions in our studies to simulate light beam propagation in hypothetical and realistic scenarios.

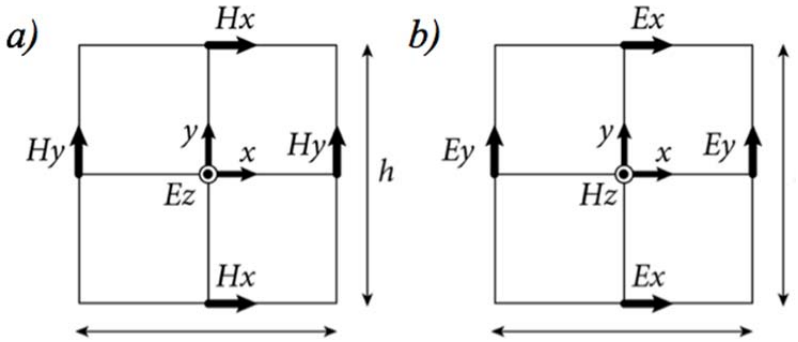

Fig. 2. Numerical representation of the 2D computational domain for a) TE and b) TM waves. Position of the fields in the 2D unit cell.

The FDTD approach is based on direct numerical solution of time-dependent Maxwell's curl equation. The FDTD algorithm as first proposed by Kane Yee in 1966 employs second-order central differences. For the calculation, the space is divided, in Cartesian coordinates, into rectangular cells which size is defined by Δx and Δy, as schematically represented in Fig. 2. In the grid, the E-field/H-field vector component is equidistant from a pair of H-field/E-field vector components, considering central difference approximation of

the derivatives of Maxwell's equations. The z direction, perpendicular to x-y plane is assumed to be infinite. The spatial confutation determines along with the spatial resolution determines the temporal time step Δt. Once the cell size is chosen, the Courant condition or the stability condition dictates the time step [Cou28]. For stability reasons, a field component cannont propagate more than once cell size in one time step.

$$\Delta t \leq \frac{\Delta x}{c_0} \qquad \text{Eq.(2.16)}$$

where it is assumed that the wave travels at c_0, the speed of light.

Yee's scheme considered Ex and Hy.

The algorithm can be summarized as follows:

1. Replace all the derivatives in Ampere's and Faraday's laws with finite differences. Discretize space and time so that the electric and magnetic fields are staggered in both space and time.
2. Solve the resulting difference equations to obtain "update equations" that express the (un- known) future fields in terms of (known) past field
3. Evaluate the magnetic fields one time step into the future so they are now known (effectively they become past fields).
4. Evaluate the electric fields one time-step into the future so they are now known (effectively they become past fields).
5. Repeat the previous two steps until the fields have been obtained over the desired duration.

There are several commercial simulation tools that implement FDTD algorithms [Crys].

Chapter 3

Beam propagation in GLM materials. High directional gain, filtering and flat lensing.

Chapter index

3.1 High directional gain in LMM

This chapter describes the first general spatial studies on beam propagation in Gain/Loss Modulated Materials (GLMM) and contains the main original contributions made to the field during my PhD research. The description follows approximately the chronological order in which they were developed. Based on four publications, two journal papers [Kum12, Kum13] and two conference proceedings [Bot11, Bot13], the chapter is divided into two main parts, the first one devoted to the high directional propagation, spatial filtering effects [Bot11, Kum12] and, the second part studies the flat lensing effect observed in Loss Modulated Materials (LMM) [Kum13, Bot13].

As pointed out in the introduction, it was originally predicted that periodic GLMM hold the ability to manage spatial diffraction of light beams [Sta09, Bot10]. The effects predicted in those pioneering works are based on the strong dependence of amplification/attenuation of electromagnetic waves on the direction of propagation within GLMM. However, these studies were based on a paraxial approximation, which therefore excluded reflection at large angles. Therefore, such results could not be directly applicable to GLMM, for modulations on the wavelength scale.

In refs. [Kum12, Kum13], we analyze the propagation of beams through GLMM using Finite Difference Time Domain (FDTD) method and prove the predicted affects. FDTD method is used to simulate propagation of light through photonics structures, and contains no simplifications. We perform FDTD analysis on structures with different geometries, being either square or rhombic, embedded in an inactive background (no gain, no loss). The results shown here are for absorptive, linear materials; however, the main conclusions still hold for general GLMMs.

As a matter of fact, losses are present in all photonic structures, and while generally neglected when designing ideal structures, they may represent a serious drawback for most actual devices. They should be considered in every system, especially when dealing with periodic structures. Hence, we shall start by the simplest case, considering purely lossy periodic structures, LMMs, with no index contrast. This will be considered as an ideal and hypothetical scenario; however,

the purpose here is to investigate whether it is possible to take advantage of inherent losses present in such structures. Also, if gain is present in the linear structure, the wave amplitude will grow exponentially to infinity. By this simplification we avoid another difficulty in managing the non-linear growth of light intensity, which in turn leads to numerical saturation.

However, the conclusions extracted from refs. [Kum12, Kum13] hold for general GLMMs. For the case of LMMs, the modes exhibiting low losses have a similar spatial distribution as the modes with highest amplification in the case of GLMMs, either with a significant net gain, or with zero net gain. The first band of a two-dimensional (2D) square GLMM with zero net gain is provided in Fig. 3.1.

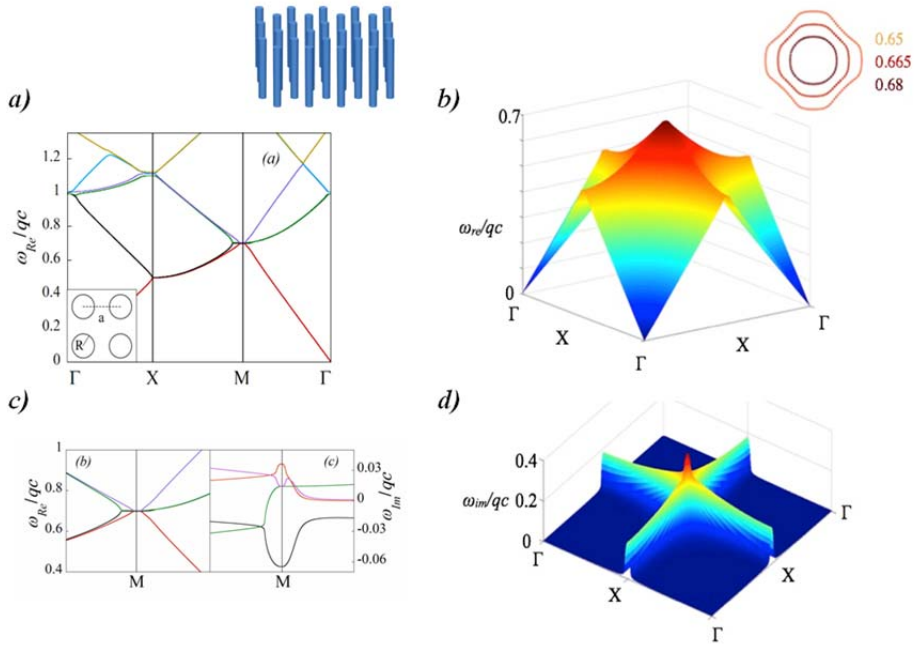

Fig. 3.1. Band diagram of a 2D square GLMM, consisting of a square lattice of gain cylinders, n=1+0.3i, of radius R=0.3a, being a the lattice constant, embedded in a lossy background medium, n=1-0.118, to provide zero net gain; see the insets of figure a). a) Real part of the band diagram, the normalized frequency is expressed in units of ω_{Re}/qc, being c the speed of light in vacuum and q the reciprocal lattice constant; Γ, M and X are the reciprocal lattice with the high symmetry points. b) Representation of the real part of the first band centered at M point. The inset shows the isofrequency contour near the resonant frequency 0.707. c) Imaginary part of the band diagram, ω_{Im}/qc, as a function of the wavevector direction. d) Representation of the imaginary part of the first band centered at M point. [Bot10]

The real part of the band structure (Figures 3.1a and 3.1b) is similar to that of an index modulated PhC [Souk12]. The major significant difference between an index modulated PhC and a LMM is the locking of modes at the *M* point, see Fig. 3.1a, and the strong amplification/attenuation close to the edge of the First Brillouin Zone (FBZ), see Fig. 3.1d. Analogously to what occurs in PhCs, the change in the curvature of the isofrequency contours close to the edge of the FBZ (see the inset in Fig. 3.1b), hints that beam spatial effects may be expected also for LMM. Note that for the normalized frequency ω_{re}/qc = 0.65, the isofrequency contour has a positive curvature, which leads to normal diffractive propagation. However, for a normalized frequency, a/λ, of 0.665 the curvature becomes flat along the ΓM direction, which corresponds to non-diffractive propagation. Finally, the negative curvature for a frequency of 0.68 may gives rise to negative diffraction. Therefore, throughout the study, we focus our interest at the edge of FBZ to demonstrate such expected spatial effects in GLMMs.

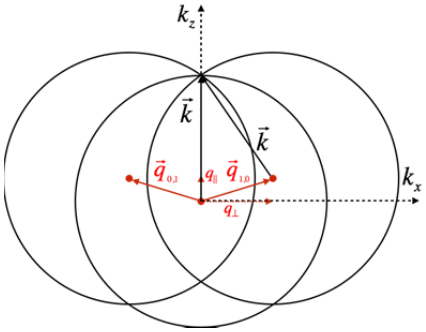

Fig. 3.2. Resonance condition for the first three modes in reciprocal space of a general rhombic lattice defined by the reciprocal lattice vectors: $\vec{q}_{0,1}$ *and* $\vec{q}_{1,0}$*. The transverse and longitudinal components of the reciprocal lattice components are denoted by* $q_{\perp}$ *and* $q_{\parallel}$ *and the wavevector is denoted by* $\vec{k}$ *.*

The edges of the FBZ may be determined geometrically, by imposing the resonance condition on the wavevector space, see the schematic representation on Fig. 3.2 for a general triangular lattice. Let us consider a lattice defined by the direct lattice vectors $\left\{\vec{a}_1 = a_{\perp}\vec{i} + a_{||}\vec{j}, \vec{a}_2 = -a_{\perp}\vec{i} + a_{||}\vec{j}\right\}$ forming an angle 2φ, so that the transverse and longitudinal components are: $a_{\perp} = a\,sin(\varphi)$ and $a_{||} = a\,cos(\varphi)$ (being therefore the transverse and longitudinal

periods of the lattice $2a_{\perp}$ and $2a_{||}$). The resonant condition for the wavevectors in the reciprocal lattice space may be then determined by:

$$k^2 = q_{\perp}^2 + (k - q_{||})^2 \qquad \text{Eq.(3.1)}$$

and, therefore:

$$k = \frac{q_{\perp}^2 + q_{||}^2}{2q_{||}} \qquad \text{Eq.(3.2)}$$

where $q_{\perp}$ and $q_{||}$ are the reciprocal lattice vectors components, as defined by: $q_{\perp} = \frac{\pi}{a_{\perp}}$ and $q_{||} = \frac{\pi}{a_{||}}$, see the schematic representation of the mode resonance in Fig. 3.2.

We investigate three different 2D LMM structures with different geometries: two rhombic and one square lattices. For both rhombic lattices determined by an angle between the direct lattice vectors in real space, 2φ, of either 75º and 105º respectively, we consider propagation along the ΓM (Fig. 3.3a) and ΓK (Fig. 3.3b) crystallographic directions. For the square lattice we study the propagation along the ΓM direction (see Fig. 3.3c). Substituting for $a_{\perp}$, $a_{||}$ and expressing the wavevector, $k = 2\pi/\lambda_{BZ}$, and further simplifying, we obtain the condition for the normalized frequency at the FBZ edge as:

$$a_{BZ} = \frac{a}{\lambda_{BZ}} = \frac{1}{2\sin(2\varphi)\sin(\varphi)} \qquad \text{Eq.(3.3)}$$

From Eq.(3.3) we may obtain the values for a_{BZ} for the square, and rhombic geometries, characterized by the angles between the lattice vectors, or equivalently between the reciprocal lattice vectors 2θ; being $2\theta=75°$ (rhombic geometry with propagation along long diagonal in direct space), $2\theta=90°$ (for the square geometry), and $2\theta=105°$ (rhombic geometry with propagation along short diagonal, in direct spce), that is to say, for propagation along the ΓM and ΓK directions. Note that $2\varphi+2\theta=\pi$. Such normalized values (a_{BZ}/a) are, respectively 0.65, 0.707, and 0.85. Figure 3.3d shows the relation between the normalized a_{BZ} and φ obtained using the above equation

for the three geometries considered throughout the chapter. Effects are expected to occur precisely at the edge of the FBZ.

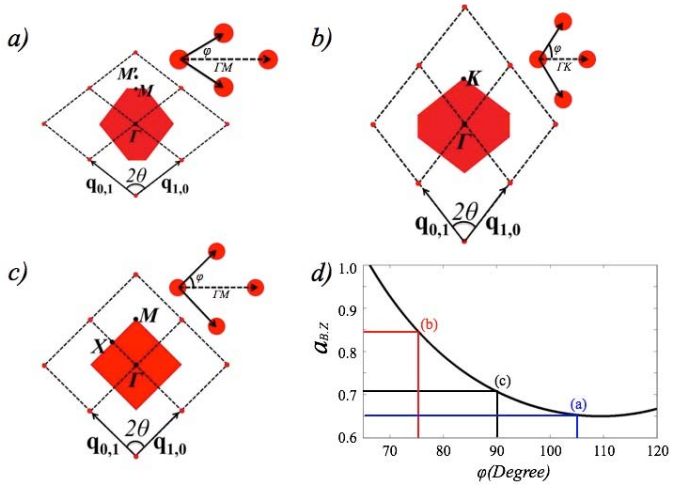

Fig. 3.3a) Schematic representation of the mode resonance to determine the M point of a rhombic lattice, referred as long diagonal. b), c) and d) show the reciprocal lattice geometry of the structures considered in the analysis. The red shaded areas indicated the irreducible FBZ. The inset shows the lattice geometry, with the dashed arrows indicating direction of propagation and the angle between two lattice vectors φ. d) Relation between a_{BZ} (normalized frequency a/λ_{BZ}) and φ; being $2\varphi+2\theta=\pi$. The lines indicate the geometries used in the analysis and the corresponding value for a_{BZ}.

3.1.1 Angular transmission profiles in LMM

In ref. [Kum12], we show that the amplification or attenuation of light waves in artificial materials may become extremely sensitive to the propagation direction when spatially modulating the gain/loss of the medium on the wavelength scale. We provide a numerical proof of such high anisotropy of the gain/loss in 2D periodic structures with square and rhombic lattice symmetry by solving the full set of Maxwell's equations using the Finite Difference Time Domain Method (FDTD), using the commercial FDTD algorithm Crystal Wave [Crys]. Precisely, such anisotropy of the amplification/attenuation leads to the narrowing of the angular spectrum of the propagating radiation with wavevector close to the edges of the FBZ. The effect may provide a novel and useful method to filter out high spatial harmonics from noisy beams.

Spatial filtering effects are therefore associated with the amplification or attenuation of specific modes. To assess the filtering performance of LMM, it is first necessary to reconstruct the angular transmission profiles of the medium. The structure considered for the FDTD analysis is a 50μm wide and 20μm long crystal made of lossy cylinders (radius $R = 0.2a$, being a the lattice constant) embedded in air. The loss considered is on the order of $10^5 cm^{-1}$. The beam waist is chosen in such a way that it covers several transverse modulations of the LMM structure. For comparison, we consider both the TE and TM polarizations of the waves. Field distributions are measured at twice the Rayleigh distance denoted by the red line in Fig. 3.4a. The obtained field distribution within the crystal and the corresponding Fourier transform, for a given frequency, are provided in Figures 3.4b and 3.5c, respectively.

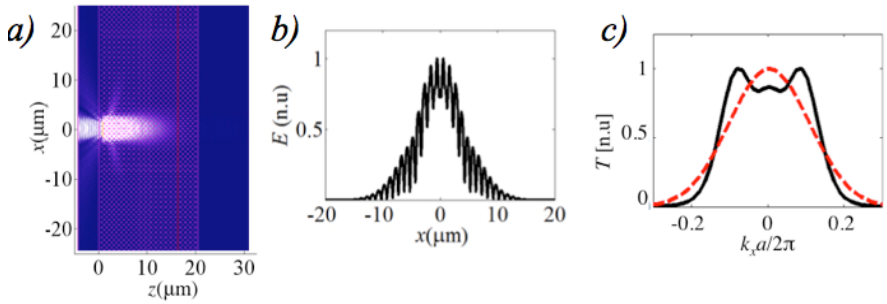

Fig. 3.4. Light propagation in a LMM with square lattice geometry. The solid red line in a) indicates the plane in which the field distribution is analyzed. The black curves in b) and c) depict the propagated field distribution and its Fourier transform. The red dashed curve in c) indicates the Fourier field distribution for the same beam propagation within a homogenous medium.

Note the symmetrically placed lobs in the Fourier spectra, in Fig. 3.4c, arising at the coupling frequencies. A transverse frequency scan in the range close the edge of the FBZ is performed, the angular transmission profile is obtained by normalizing the Fourier spectra with that of the beam propagated through a homogenous medium.

The analysis of both TM and TE polarizations (see Fig. 3.5), demonstrated that this spectrum narrowing effect is more pronounced in the case of TM polarization, i.e. when the electric field polarized parallel to the rods. The edge of the FBZ for a square lattice corresponds to a_{BZ} =0.707. The two equally spaced lobs converging at the edge of the FBZ perfectly match the PWE analysis.

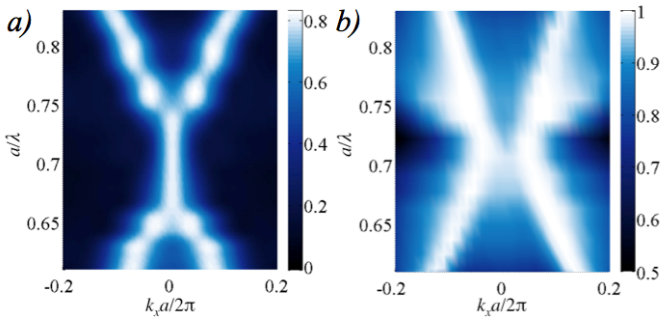

Fig. 3.5 Angular transmission profiles obtained from the normalized Fourier spectra in a/λ units for both the parallel a) and the perpendicular b) polarization in a square LMM crystal.

3.1.2 Spatial filtering in LMM

From the angular transmission profile, it can be seen that close to edge of the FBZ, only the central range of frequencies is amplified (or less absorbed). This fact may become a useful tool for spatial filtering as it means that the surrounding frequencies of a noisy signal can be easily filtered out.

While reconstructing the angular transmission profiles, we observe that the narrowing of the Fourier spectrum is still enhanced in the case of a rhombic geometry, and especially for propagation along the long diagonal, see Fig. 3.3.a. Therefore, we propagate a random noisy beam along ΓM direction of the rhombic LMM crystal and the results clearly show the expected spatial filtering effect.

Figure 3.6 shows the spatial filtering performance from a rhombic LMM. In Fig. 3.6b a comparison of the spectral components of the input noisy beam and filtered beam is provided. Note that the filtered output contains an amplified central frequency. Besides, Fig. 3.6c shows the response of the LMM for a noisy beam input, where, at the edge of the FBZ (a_{BZ}=0.85 for the considered rhombic structure), only the central part of the frequency is amplified.

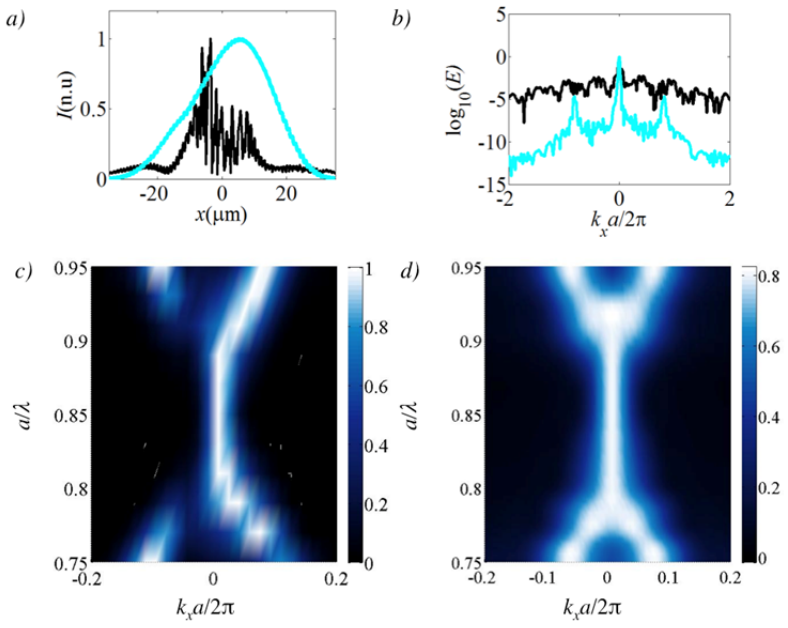

Fig. 3.6 a) Input noisy beam (black) and filtered output beam (green) intensities. b) Corresponding Fourier spectra of the incident noisy beam and filtered output. Angular transmission profiles of the rhombic lattice structure, for the two input beams: c) noisy beam and d) Gaussian beam.

3.2 Flat lensing in LMM

Flat lensing is accounted by convex-curved isofrequency contours of propagating modes in wavevector space. The effect arises as convex phase shifts are accumulated through either a negative-index material [Pen00] or a PhC slab [Luo02, Cub03, Ber04], and are further compensated by normal diffraction beyond the structure, determining the focalization distance from the flat lens.

In this study [Kum13], we propose a flat lensing effect using a periodic loss-modulated material. The effect is analytically predicted by the dispersion curves obtained from the coupled mode expansion of Maxwell Equations and further confirmed by numerical beam propagation simulations. From both, analytical and numerical studies, we concluded that, for a range of frequencies, light beams undergo negative diffraction on propagation through the loss-modulated medium, leading to a window of high transmission. The phase shifts accumulated by negative diffraction within the structure are then compensated by normal diffraction, leading to substantial

focalization beyond it. Figure 3.7 provides a schematic representation of the focusing performance by a LMM. At given frequencies, the beam undergoes negative diffraction within the crystal, while spreading, the curvature of wave fronts becomes concave. Then, propagation in free space with normal diffraction compensates such curvature of the phase fronts leading to the flat focusing effects

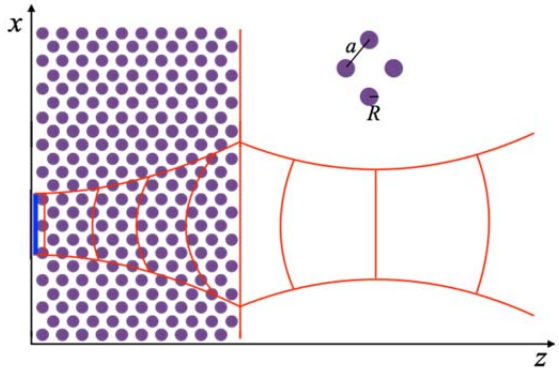

Fig. 3.7. Schematic representation of beam propagation in a LMM structure. The Gaussian source is shown as blue line. The inset shows the unit cell.

3.2.1 Negative Diffraction. Numerical analysis

In order to show the flat lensing effect by a LMM, we assume a 2D medium with a harmonic periodic modulation of the complex refractive index. Once again, we consider square and rhombic lattices.

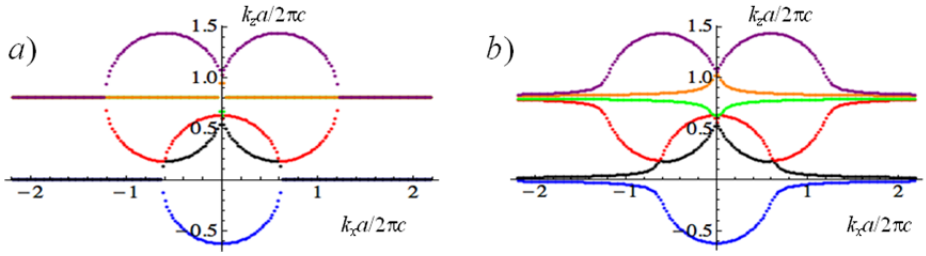

Fig. 3.8. Mode coupling of three adjacent dominant modes in a structured LMM with rhombic geometry, k_z as a function of k_x, where $\vec{k}=(k_x,k_z)$. The three adjacent modes are represented by three uncoupled circles in a). The resonance point where three modes intercept is shown in b) for a homogenous media and d) for LMM.

The system can be described by using three adjacent modes in the mode expansion [Kum13]. For a perfect homogeneous medium, the dispersion of each mode corresponds to a circle in wavevector space which radius increases with frequency. Figure 3.8 depicts the dispersion for frequencies falling before and after resonance. The perturbed three resonant modes in wavevector space for a structured LMM intersecting at the edge of FBZ are shown in Fig. 3.8b.Therefore, the character of diffraction can be directly determined by means of the curvature of the dominant mode of the spatial dispersion (real part of the normalized longitudinal wavevector k_z as a function of k_x, where $\vec{k}=(k_x,k_z)$, at k_x=0).

For normal diffraction, the curvature of dispersion is positive, as in Fig. 3.9a. For negative diffraction, the dispersion curve acquires negative curvature as in Fig. 3.9b. In both cases the beam spreads while propagating, see Figs.3.9b and 3.9d.

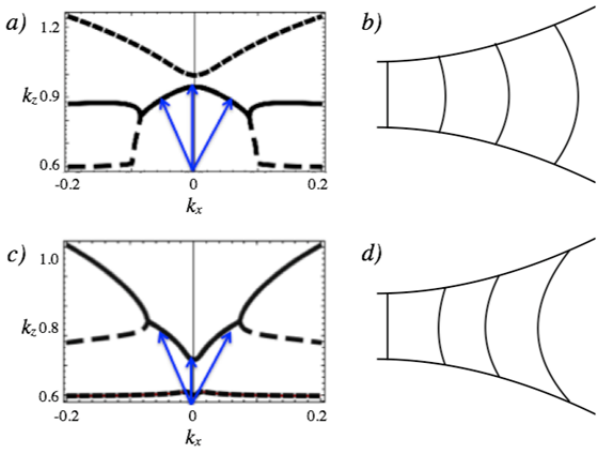

Fig. 3.9. Mode coupling of three adjacent dominant modes in a structured LMM. The dominant mode is represented by the bold curve. Blue lines denote the propagation wavevectors. a) Coupling leading to normal diffraction. c) Coupling leading to negative diffraction. The plots on the right column schematically represent the diffractive broadening in both case.

From the analytical studies [Kum13], coupled mode analysis, the analytical curvature,κ, may be determined as the second derivative of the longitudinal wave number with respect to the transverse component, across the edge of the FBZ (where the change of curvature, see Fig. 3.1b). Considering a general form: $k_z = f(k_x)$, the curvature of the dispersion may be obtained as:

$$\kappa = \frac{\frac{d^2 k_z}{dk_x^2}}{\left(1+\left(\frac{dk_z}{dk_x}\right)^2\right)} \qquad \text{Eq. (3.4)}$$

Assuming the slope, $\frac{dk_z}{dk_x}$, small as compared to unity,κ becomes $\frac{d^2 k_z}{dk_x^2}$.

Figures 3.10a and 3.10b depict the complex mode coupling for rhombic LMM and propagation along the long diagonal. While the real part of dispersion determines diffraction, the imaginary part, k_{im} accounts for absorption. The analytical curvature of the dominant mode, the less absorbing one, is determined as a function of the frequency in Fig. 3.10c. Such curvature can then be compared to the phase evolution obtained from numerical propagation studies.

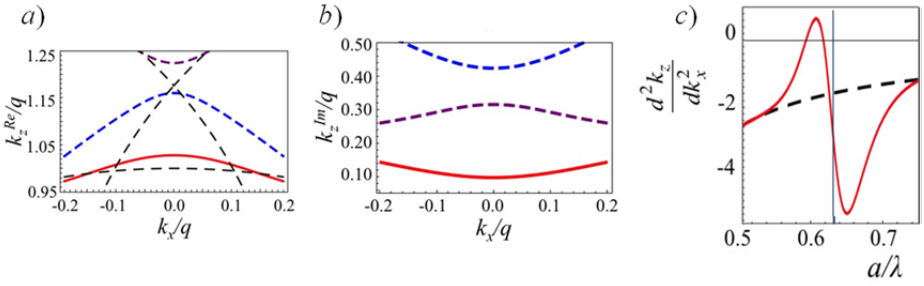

Fig. 3.10. Complex dispersion, a) real and b) imaginary, and corresponding diffraction, c), for a rhombic geometry LMM, along the long diagonal.

3.2.2 Numerical Lensing Analysis.

In order to confirm the different diffractive regimes, we numerically propagate light beams using FDTD. We may consider a LMM structure and propagate a Gaussian beam within it with central carrier frequency close to the edge of the FBZ. Then, we numerically evaluate the phase profiles at a given exit plain. For a range of frequencies, a/λ, on either side of FBZ, the phase profiles are obtained after propagation through the LMM crystal. We consider a 15-period long structure, with lossy cylinders embedded in air. The complex refractive index of the cylinders is fixed to be 1+0.4i (corresponding to an absorption coefficient of α = 5 x 10^4 cm^{-1}). The radius of the cylinders, R, is considered to be R = 0.2 a, where a stands for the lattice constant. We here provide the example of the study of a rhombic geometry, 2θ=105°, for propagation along the

long diagonal of the reciprocal space. We consider a Gaussian beam, width of 1.5 μm, and given central carrier frequency close to the *K* high symmetry point, incident on the structure; we numerically evaluate the phase profiles at a given exit plane. The layout of the numerical grid is depicted in Fig. 3.11. The excitor is placed inside the LMM, with a detector, D1, at the exit plane of the structure. Another detector, D2, is located at 30 μm from the exit plane and a third detector, D0, at x=0, provides the horizontal cross section of the field. The amplitude and phase of the electric field is determined at all detectors.

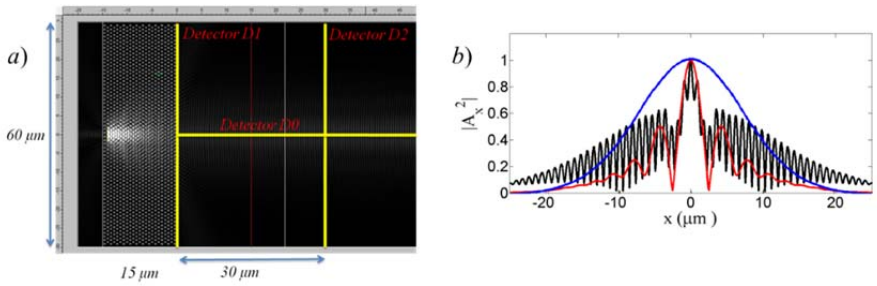

Fig. 3.11 a) Representation of the FDTD calculation scheme indication the position of the detectors D0, D1 and D2. b) Incident field (blue curve), field at detector D1 (black curve) and at detector D2(red curve).

Figures 3.12b and 3.12c present the different curvatures of the phase associated with frequencies a/λ =0.62 and 0.7, for propagation along the long diagonal of a rhombic lattice (resonant frequency for the structure, i.e. edge of the FBZ corresponding to a/λ=0.63). The phase of the propagating beam is obtained from the electric field at D1. The curvature of the phase is calculated using Eq. 3.4. From Figures 3.12a and 3.12b it can be noted that the phase curvature dependence on the carrier frequency obtained from numerical simulations, reproduces the analytical curvature. For all the structures considered in [Kum13], the analytical and numerical predictions show a good agreement.

While for frequencies far from the FBZ edge, the phase curvatures would resemble the reference beam, near resonance, propagating within the LMM strongly deviates from the reference beam, see Figs. 3.12b and 3.12c. The transition from negative to strong positive diffraction occurs precisely at the resonant frequency.

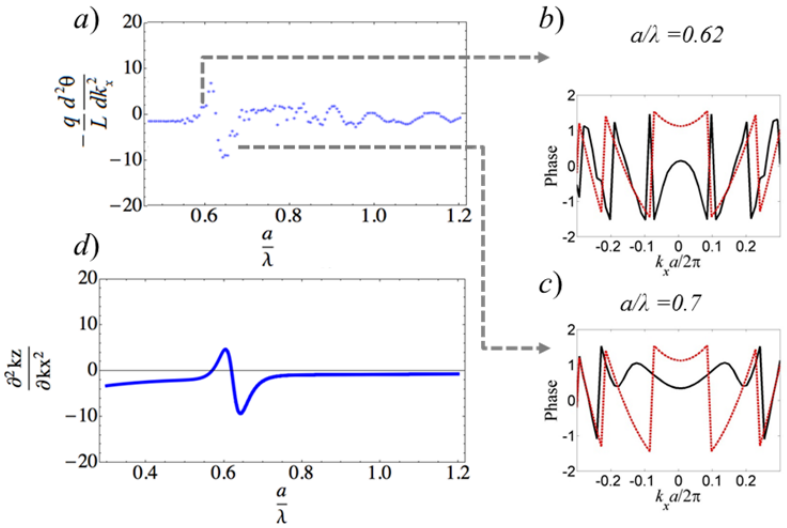

Fig. 3.12 a) Analytical dispersion curvature plotted as a function of the carrier frequency, in a/λ units, for propagation along the short diagonal of a rhombic structure. The dashed curve corresponds to the curvatures of the reference beam propagating in an equivalent homogenous medium b) Phase curvature reconstructed from the numerical modeling. The dark discontinuous lines represent the phase curvatures of the reference beam propagating. c) and d) show the phase of the beam obtained after propagation for a/λ=0.62, 0.7. The red curves in c) and d) indicate the phase curvature of the reference beam at the corresponding frequencies.

Analyzing the numeric intensity maps after the LMM, shown in Fig. 3.13, focalization is observed coinciding with a high transmission window for frequencies close to the edge of FBZ. This is a direct consequence of the anisotropic attenuation of LMM structures.

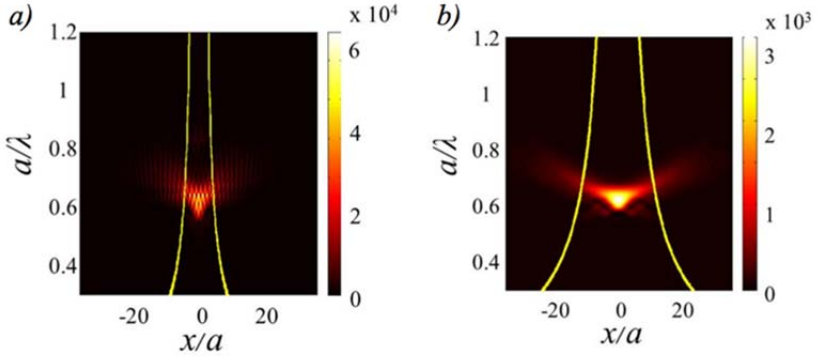

Fig. 3.13 a) Intensity transmission map for propagation along the long diagonal of a LMM, as obtained at the exit plain of the structure, and b) at a distance of 36a from the exit plain. The yellow line represents the width of the reference beam.

3.2.3 Flat Lensing in a Sonic LMM

The effect of loss modulation on beam propagation can be extended to acoustic regime as well. In [Bot13] we compare beam propagation in LMMs in both optical and acoustic wavelength range. We considered structures with square geometry, i.e. propagation along ΓM direction. Finite Element Method (FEM) is used for numerical simulations in acoustic LMM. A similar structure to that of LMM in optical regime analysis is consider for phononic case also. The radius of absorbing cylinders are fixed at $R=0.2a$ and the extinction coefficient of $\alpha=1.37$.

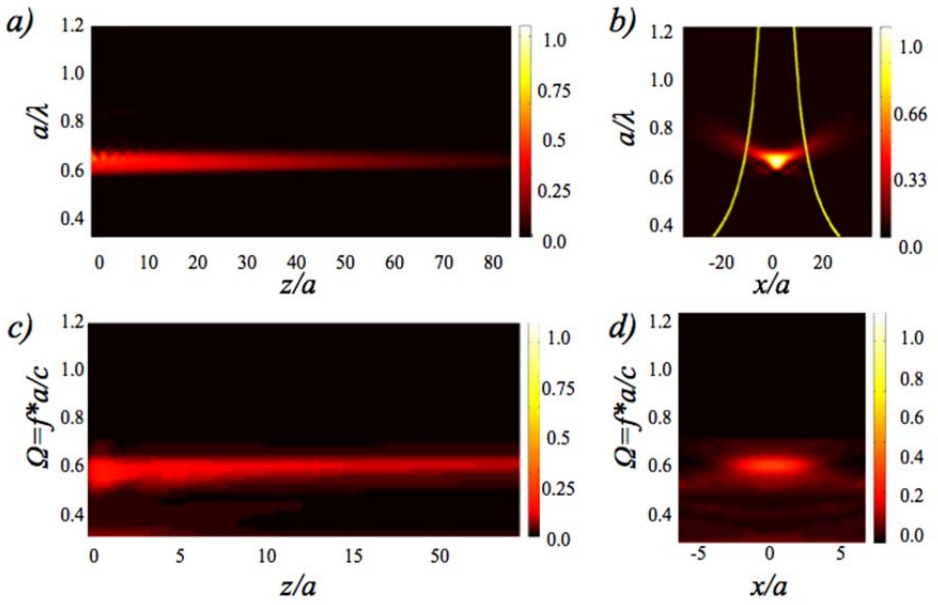

Fig. 3.14*a) FDTD transmission map for cylinders with n_{cyl} = 1+0.4i, the vertical axis denotes the carrier frequency, in a/λ _units, of the 1.5 μm-wide incident Gaussian and the horizontal axis the normalized distance from the sample. b) Transverse cross section at a distance of 36a after the structure, denoted by D in figure a), where the continuous the red dotted curve is for comparison with propagation in free space. Figures c) and d) show analog numeric FEM calculations for a sonic crystal made of cylinders with extinction, α =1.37, embedded in air.*

Figures 3.14a and 3.14c compare the intensity distribution along the horizontal axis of propagation. The presence of a high transmission window around the edge of the FBZ (Ω =0.707) can be seen in both optical and acoustic regimes. A small degree of focalization can also be observed to frequency close to a/λ=0.65.

Publication I

[Bot11] M. Botey, R. Herrero, N. Kumar, R. Vilaseca, and K. Staliunas, *"Self-collimation and spatial filtering in 2D gain/loss periodic spatially modulated materials",* in European Quantum Electronics Conference (p. EI_P8) Optical Society of America (2011) [Bot11]

Self-collimation and spatial filtering in 2D gain/loss periodic spatially modulated materials

Muriel Botey[1], Ramon Herrero[2], Nikhil P. Kumar[2], Ramon Vilaseca[2], Kestutis Staliunas[3]

1. EUETIB. Departament de Física i Enginyeria Nuclear, Universitat Politècnica de Catalunya, Barcelona, Spain, EU
2. Departament de Física i Enginyeria Nuclear, Universitat Politècnica de Catalunya, Terrassa, Spain EU
3. ICREA, Departament de Física i Enginyeria Nuclear, Universitat Politècnica de Catalunya, Terrassa, Spain, EU

We predict and demonstrate that the periodical modulation of the gain/loss profile on the wavelength scale in at least two dimensions of space can lead to interesting beam propagation effects, similar to self-collimation or subdiffractive propagation, but also to spatial beam filtering.

While in photonic crystals (PCs) the modulation of the refractive index brings about the formation of band gaps in the frequency dispersion spectra, the seemingly analogous materials, those with gain/loss modulation (GLM) do not exhibit such celebrated property. However, it has been recently shown that the GLM on the wave scale in 2D systems may also strongly modify the propagation properties of waves both in time and space domains. In this case, the modification of the spatial dispersion can lead to a variety of nontrivial effects. Whereas the refractive index modulation pushes the frequencies of the harmonic field components one from another opening the band gaps around their cross points, gain/loss modulation (GLM) has the opposite result. Indeed the self-collimation effects in PCs appear due to the deformation (flattening) of the interacting (mutually pushing) spatial dispersion curves [1]. In the case of GLM, the spatial dispersion curves become also substantially modified due to the mode pulling and locking, and thus also self-collimation effects or even negative diffraction can be expected [2]. Besides, the highly directional gain provides a beam filtering mechanism.

These propagation effects may be predicted from the plane-wave complex isoline calculations and can be mathematically rigorously derived considering the interaction of two field components in a 2D weak harmonic GLM under the paraxial approximation [3]. Finally, full numerical simulations may be obtained from FDTD field propagation computations.

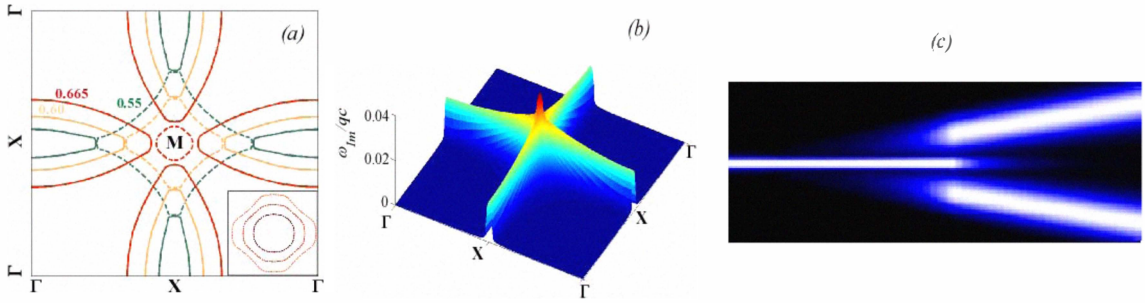

Fig. 1 *(a)* Isofrequency lines at the edge of the FBZ for a square 2D system made of cylinders ($R = 0.3a$, where a is the distance between cylinders) with gain ($\varepsilon = 1+0.3i$) embedded in a lossy medium; with no net average gain. The inset shows the curvature change close to the M high symmetry point. *(b)* Gain profile (imaginary part of the frequency) of the lower order mode around the edges of the FBZ. *(c)* Propagation of a Gaussian beam in a self-collimation regime (the sidebands, however, start growing after longer propagation, due to the additional sideband-growing effect)

References

[1] H. Kosaka et al., Applied Physics Letters 74, 1212, (1999); D. N. Chigrin et al., Optics Express 11, 1203, (2003); R. Illiew et al., Applied Physics Letters 85, 5854 (2004); D. W. Prather et al., Optics Letters 29, 50 (2004). K. Staliunas and R. Herrero, Physical Review E 73, 016601, (2006).
[2] K. Staliunas, R.Herrero, R.Vilaseca, *Physical Review A* **80**, 013821, (2009).
[3] M. Botey, R.Herrero, K.Staliunas, *Physical Review A* **82**, 013828 (2010).

Publication II

[Kum12] N. Kumar, M. Botey, R. Herrero, and K. Staliunas *"High-directional wave propagation in periodic loss modulated materials"* Photonics and Nanostructures-Fundamentals and Applications **10**.4, 644-650 (2012)

Publication III

[Kum13] N. Kumar, M- Botey, R. Herrero and K. Staliunas, *"Flat lensing by periodic loss-modulated materials",* Journal of the Optical Siciety of America B **30** (10) 2684-2688 (2013)

ATTENTION ¡
Pages 56 to 60 of the thesis are available at the editor's web
https://www.osapublishing.org/josab/abstract.cfm?uri=josab-30-10-2684

Publication IV

[Bot 13] M. Botey, N. Kumar, R. Herrero, L. Maigyte, R. Pico, and K. Staliunas, *"Negative diffraction by a periodically modulated loss"*, Transparent Optical Networks (ICTON), 2013 15th International Conference on. IEEE, (2013)

ATTENTION ¡
Pages 61 to 65 of the thesis are available at the editor's web
http://ieeexplore.ieee.org/document/6602994/

Chapter 4

Beam shaping in Metallic Photonic Crystals

Chapter index

4.1 Metallo-dielectric Photonic Crystals

In the previous chapter, we have considered Gain Loss Modulated Materials (GLMMs) or more precisely Loss Modulated Materials (LMMs) which essentially represent a limiting case of GLMMS. However, actual periodically structured materials show both refractive index and gain/loss variations, as they are intrinsically related via the Kramers–Kronig relations. Pure index modulations may only occur for given frequencies, whereas purely gain/loss modulations are barely possible. Therefore, in real materials, such two extreme (ideal) cases may never be achieved.

This chapter describes two publications, one journal paper [Kum14] and a conference proceeding [Bot14] where we study light beam propagation in systems holding both index and gain/loss modulations. The paper [Kum14] is precisely devoted to provide a detailed analysis of light beam propagation in metallic photonic crystals (MPhCs), consisting of gold cylinders embedded in air, where, indeed, both losses and refractive index are simultaneously modulated. We are able to predict and numerically prove that such a structure supports non-diffractive (self-collimated) propagation associated to zero diffraction. In this case, the lack of phase shift among transverse modes maintains the beam profile unchanged along the crystal. We also predict flat lensing associated to negative diffraction. In the latter case, the anomalous phase shifts accumulated within the structure, when compensated by normal diffraction behind it, lead to a significant focalization of light beams.

Prior to the appearance of the two publications presented here, the topic of flat lensing was usually discussed in association with left-handed materials or Negative Index Materials (NIMs). The concept of NIM was introduced by Veselago [Ves68]. He proposed that homogenous materials with negative electric permittivity and magnetic permeability would give rise to negative refractive index, thereby exhibiting anomalous propagation effects such as that light propagates with opposite phase and energy velocities; the so-called left-handed media. Such materials do not occur in nature, and therefore the study remained at a theoretical level till the advent of metamaterials: artificial electromagnetic structures engineered on subwavelength scales to tailor its response, proposed by Pendry

[Pen99, Pen00]. He suggested that artificially tailored materials, with periodically aligned metallic structures with periods smaller than the wavelength of light could present an averaged negative electric permittivity and negative magnetic permeability. These studies predicted the ability of such materials to focus electromagnetic waves to a spot size much smaller than the wavelength. These materials are better known as perfect lenses. Flat lensing was first experimentally demonstrated for metamaterials with centimetre-scale features at microwave frequencies [Sel01], and later observed optical wavelengths [Xu13].

Another fundamental advantage of flat lenses is the lack of optical axis. Conventional lenses need a curved surface to focus the electromagnetic waves, whereas a NIM can form an image with a flat surface, a trait that can be attributed to negative index of refraction. This kind of tailored materials with average negative electric permittivity and magnetic permeability are known as metamaterials. Diffraction limited imaging methods employing metamaterials have been demonstrated in microwave [Grb04, Lag04] and visible frequency ranges [Xio07, Smo07]. The fabrication of metamaterials is extremely hard considering complex nanostructures, especially in the visible range of frequencies, as the period should be the size of several nanometers.

Negative diffraction observed in PhCs is due to a very different phenomenon. It can be explained by the bends in isofrequency contours of spatial dispersion curves. In the case of PhCs, the refractive index of the material is positive, so is the electric permittivity and magnetic permeability. Investigations on the spatial dispersion relations of PhCs led to the discovery of novel spatial propagation effects as: self-collimation due to the flattening of the curvature of spatial dispersion [Kos99b, Wit02, Chi03, Aug05, Sta06, Lu06, Lom06]; spatial filtering due to the angular gaps in dispersion curves, or strongly tilted segments [Sta09a, Mai10] (as described in Chapter 2); and finally focalization and imaging behind a PhC [Luo02a, Luo02b, Li03, Luo03, Wan04, Fab06, Ren07] due to the convexly curved segments of the spatial dispersion.

The purpose of our study is to show the effect of negative diffraction on beam propagation, providing a significant focalization. In addition, we numerically demonstrate the spatial filtering of noisy

beams due to the anisotropic attenuation of light. This effect, which arises due to anisotropic gain/loss profile in GLMM– like materials, was described in an ideal scenario of pure loss modulation in [Kum12].

For this study, we consider a 2D periodic structure made of gold cylinders in air, see Fig. 4.1a. The geometry of the structure is defined by the lattice constant *a*, the angle between the two lattice vectors θ, and the radius of the cylinders *R*. The dielectric constant of dielectric materials for frequencies larger than the plasma frequency, ω_p, may be described by the Drude model, by the following expression: $\varepsilon(\omega)=1-\omega_p^2/(\omega^2-i\gamma\omega)$, where ω is the frequency of light, and ω_p stands for the collision frequency of gold [Bor80]. The absorption coefficient of Gold (Au) at $\lambda=1\,\mu m$ is $\alpha \sim 770000$ cm^{-1} and for Platinum (Pl) is around 710000 cm^{-1}.

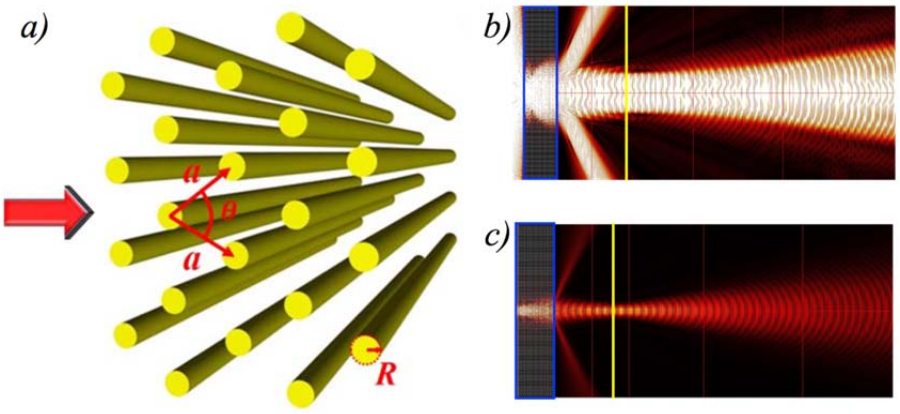

Fig. 4.1a) Arrangement of metallic cylinders embedded in air in a MPhC, a being the lattice constant, R the radius of the cylinders, θ the angle between the two direct lattice vectors indicated by thin arrows, and the thick red arrow indicates the direction of propagation of beam. b) /c) FDTD propagation of a Gaussian beam through the structure made of Platinum/ Gold cylinders respectively, R=0.2a θ =75º, The Gaussian beam carrier frequency is a/λ = 0.85. The blue rectangular boxes indicate the position of the MPhC. The yellow line is the detector, at t focus.

We numerically propagate a Gaussian beam using Finite Difference Time Domain (FDTD) method. The electric field considered is linearly polarized parallel to the cylindrical rods. The field intensity distribution of a Gaussian beam of width 3μm propagating through MPhCs with periodically arranged Platinum (Pl) and Gold cylindrical rods are depicted in Figures 4.1b and 4.1c. The length of the crystal is 9 periods, around 10 μm. The geometry of the structure is defined by

the angle between direct lattice vectors, θ, which is 75º, i.e. we are considering propagation along the long diagonal of the rhombic structure, along the ΓM direction, —as spatial effects are generally enhanced in such rhombic structure as compared to square geometry [Kum12, Kum14]—. From the figures it can be seen that, for a particular frequency (a/λ = 0.85) focalization of the beam after propagation through the crystal occurs in both cases, either for Au or Pl MPhCs, but being the effect stronger for the case of Au cylinders.

The spatial propagation effects may be interpreted using isofrequency contours. In Fig. 4.2, we try to predict the behavior of light beam using the band diagrams of two consecutive bands. Fig. 4.2b corresponds to the isofrequency curvatures for the low-lying band, i.e. a/λ=0.56-0.83 and Fig. 4.2c for the higher band with frequency range a/λ=0.83-1.1.

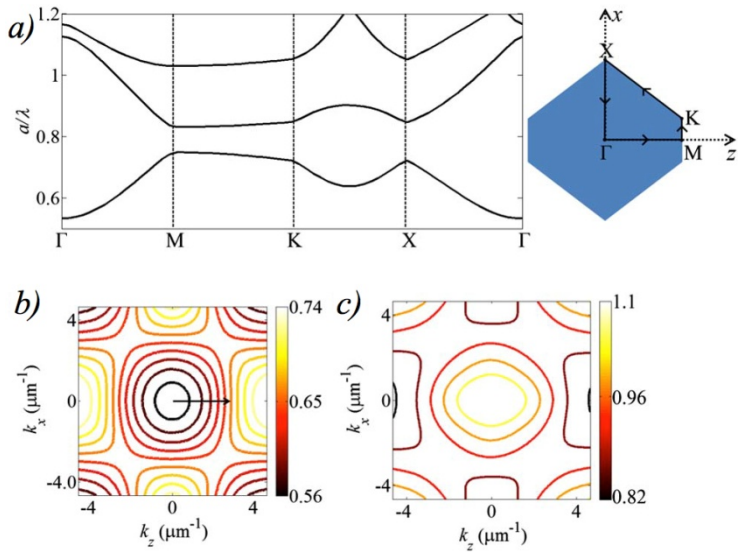

Fig. 4.2 a) Band diagram for the rhombic structure with θ = 75º. The irreducible First Brillouin Zone (FBZ) is shown in the offset, with the high symmetry points and arrows indicating directions for calculation of the band. b),c) Isofrequency contours for two consecutive bands lying below and above the bandgap. The colorbar indicates the frequency in a/λ units.

The curvature of the spatial dispersion, see 4.2b, becomes flat for frequencies close to a/λ=0.68; accounting for non-diffractive propagation. Increasing frequency, increasing the arrow indicating the direction of propagation, the dispersion curve becomes convex with respect to the direction of propagation for the range of

frequencies, 0.68 < a/λ < 0.74. This negative diffraction may lead to the focusing of beams after propagation trough the MPhC.

From the isofrequency contours of the higher band, Fig. 4.2c, we can predict similar effects. At a/λ = 0.83, there is a transition from convex to concave curvature. There, a non-diffractive regime is expected. This effect may not be as pronounced as the one expected for the lower band, owing to the smaller angular frequency coverage as observed from the figure. On the other hand, a significantly pronounced negative diffraction is expected for frequencies a/λ > 0.84, due to: i) a larger coverage of angular spectrum, and ii) a stronger curvature of the spatial dispersion.

In order to optimize the computational time, we numerically propagate a Gaussian beam through the MPhC structure, and feed the resultant amplitude and phase information as input to a paraxial propagation model. The value of the filling fraction $f = R/a$ is optimized to obtain the maximum focalization after propagation through the MPhC. Therefore, assuming for all calculations an input beam frequency fixed to be a/λ = 0.85 we analyze the focalization performance for different values of the filling fraction.

The intensity map of the horizontal cross section detector and the intensity distribution for a vertical detector at the focal plane, Figures 4.3a and 4.3b, indicate the best focusing occurring for f = 0.2; as already previously observed [Kum13, Kum14].

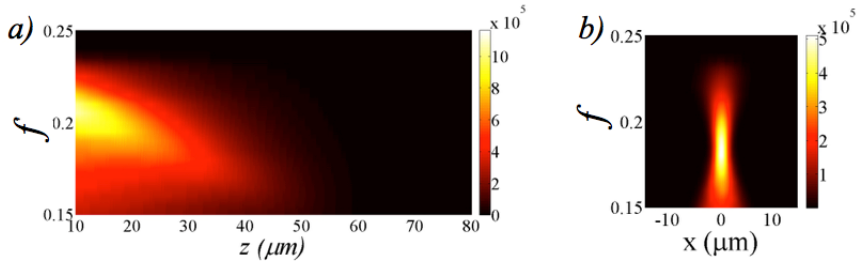

Fig. 4.3. a) Intensity distribution in z, for propagation along the ΓM direction and a/λ=0.85, for different filling fraction f. b) Intensity distribution at the focal point.

4.2 Non-diffractive propagation in Metallic Photonic Crystals

Non-diffractive propagation within a MPhC is associated to the in-phase propagation of all angular components of a beam. Then, the spatial shape of a beam is preserved as the angular components

propagate with the same phase velocity, as schematically illustrated in Fig. 4.4a. In a MPhC, it is possible to propagate a beam almost without distortion when its carrier frequency corresponds to non-diffractive regime, resulting in collimated propagation within the crystal.

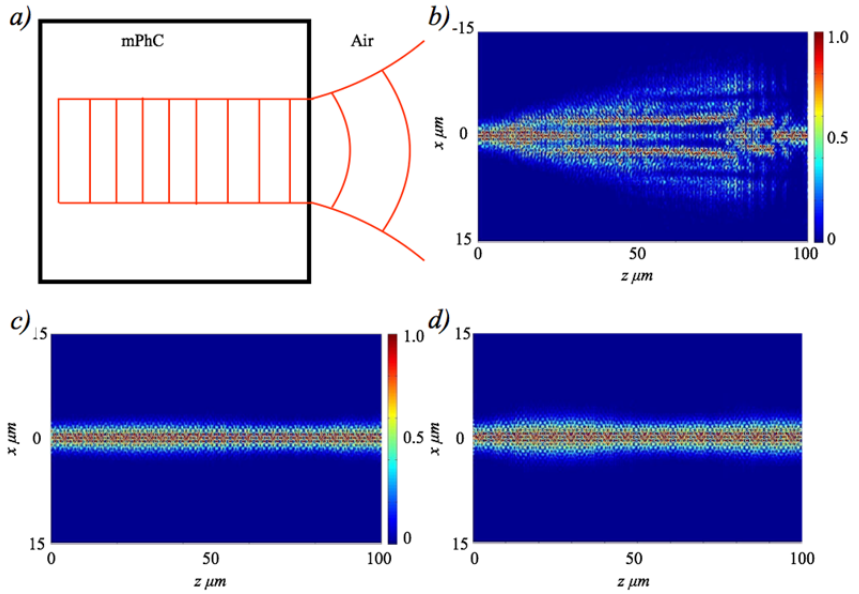

Fig. 4.4 a) Geometrical interpretation of diffraction of a Gaussian beam in air, and self-collimation inside the crystal. b) Normal diffraction of a Gaussian inside the MPhC crystal of Fig. 4.2 with carrier frequency a/λ = 0.64. c) Non-diffractive propagation at a/λ = 0.7. d) Propagation at a higher frequency a/λ = 0.72. The intensity is normalized to unity at every x-plane (vertical cross sections as the intensity decreases exponentially due to losses) for the sake of visualization.

We now consider the arrangement of metallic rods in a rhombic geometry of Fig. 4.2 and propagation along ΓM. While for low frequencies the beam undergoes normal diffraction within an, see Fig. 4.4b, increasing frequency the structure supports self-collimated propagation, see Fig. 4.4c. Finally, further increasing frequency, we may find regimes of anomalous diffraction, see Fig. 4.4d, which will be later discussed in detail.

In fact, for the same MPhC there may be different self-collimation regimes, as shown in Fig. 4.5a and 4.6b. Fig. 4.5a corresponds to a frequency of a/λ = 0.68 and to a/λ = 0.79. While both frequencies correspond to flat segments in the spatial the angular coverage of such the flat segment is larger in the first case. The loss experienced by the Gaussian beam upon propagation through the structure is

similar in both cases as indicates the cross-section of the intensity profile depicted in Figs 4.5c and 4.5d, respectively.

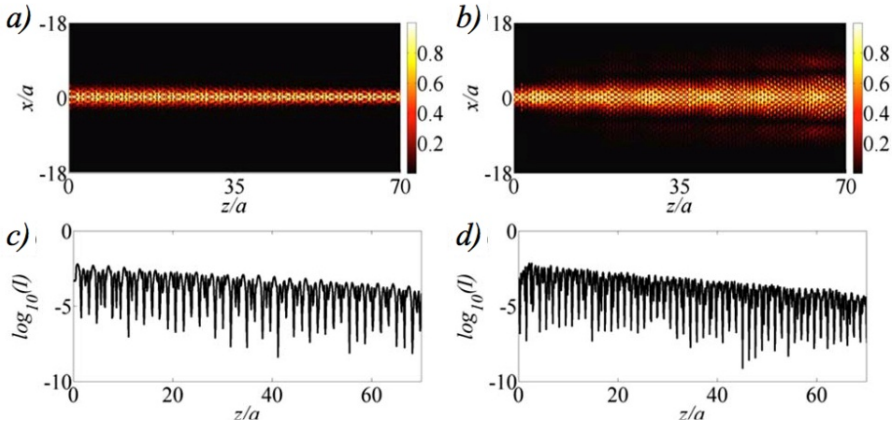

Fig. 4.5. *Non-diffractive propagation inside an infinite MPhC with the same structural parameters of Fig. 4.2. a) Normalized intensity profile of the propagated beam in a length of 70a considering an initial beam of width 2.5a, at: a) a/λ = 0.68; b) at a/λ = 0.79. c)/d) Corresponding horizontal cross sections of the intensity profile corresponding to x = 0.*

4.3 Negative diffraction in Metallic Photonic Crystals

As already shown, MPhCs may support anomalous or negative diffraction, for different ranges of frequencies. The first of these ranges lying just below the resonant frequency. A Gaussian beam propagating through an MPhC may accumulate a strong negative phase which, at some point after exiting the MPhC, is compensated by free space propagation. All the angular components become in-phase at the focal point.

The anomalous diffraction leads to the flat focusing effect as schematically represented in Fig. 4.6a. This is supported by MPhC with rhombic or square geometries, as in Fig. 4.6b. Note that the focal distance is determined by the curvature of spatial dispersion. A higher the curvature of the dispersion leads to a larger focal distance, since the negative phase accumulated in propagation within the crystal required a larger propagation distance behind the crystal to compensate it. Such curvature, and hence the corresponding focal length are strongly dependent upon frequency.

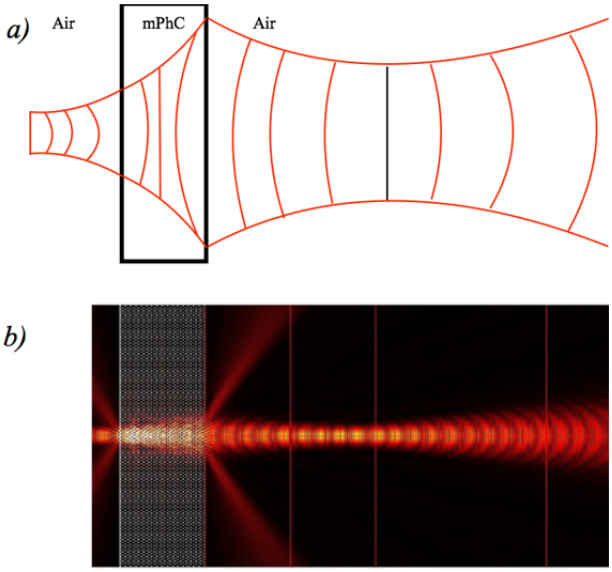

Fig. 4.6.a- Geometrical interpretation of a Gaussian beam undergoing anomalous diffraction on passing through a periodically loss modulated structure b) Propagation of a Gaussian beam of carrier frequency a/λ = 0.6 through the MPhC.

Such frequency dependence on the focal distance is analyzed Fig. 4.7a, for a square geometry (edge of the FBZ at a/λ = 0.707). Flat focusing is observed as the frequency increases below the resonant frequency, from a/λ = 0.6 to a/λ = 0.7. The curvature of spatial dispersion increases with frequency, as focal length increases. This can be shown representing the peak intensity of the on-axis intensity profile, see Fig. 4.7b.

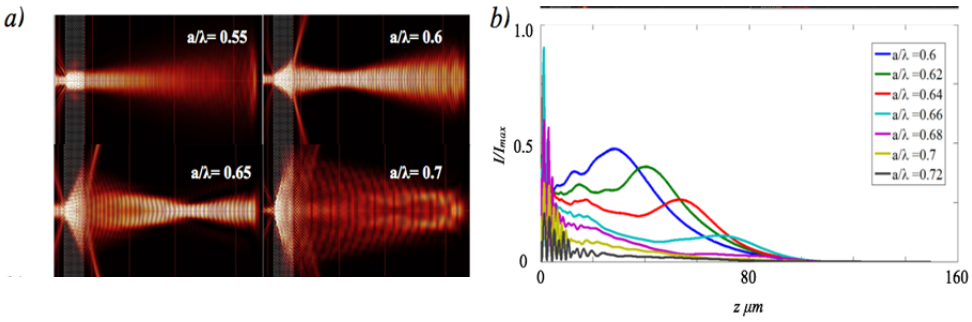

Fig. 4.7 a) Negative diffraction in a MPhC with square geometry for different carrier frequencies a/λ = 0.55, 0.6, 0.65 and 0.7 below the resonant frequency. b) On axis intensity profiles for a range of frequencies a/λ = 0.6-0.72.

Also, the width of the beam at the focal point varies with the number of periods, length of the MPhC crystal. The beam waist becomes narrower as the number of periods increases from 5 (Fig. 4.8b) to 9

(Fig. 4.8f); in this case the analyzed structure is of rhombic geometry with propagation along long diagonal.

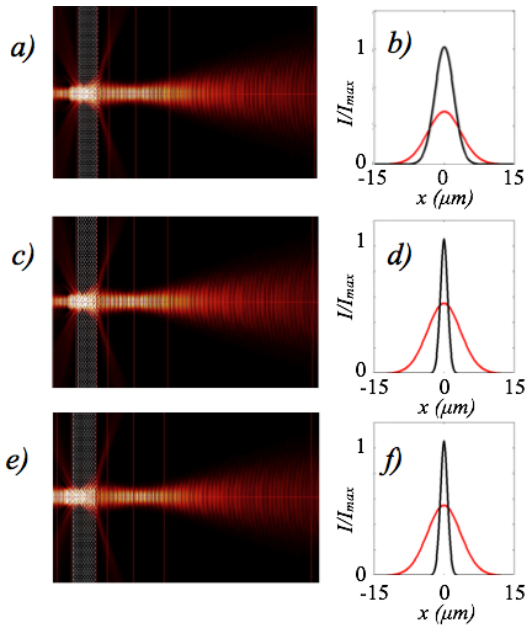

Fig. 4.8. Left column: negative diffraction in MPhC with different number of periods: a) 5, c) 7 and e) 9, respectively. Right column: intensity profile of a Gaussian beam at focus (black solid curve) in comparison with the intensity profile of a beam propagating in free space.

A detailed study was carried out for different structural geometries [Kum14]. Figure 4.9 presents the horizontal cross section (at z=0) of the normalized intensity of a Gaussian beam propagating along the long and short diagonal through a rhombic (parameters of Fig. 4.2c) MPhC a comparison between propagation of a rhombic structure. two significant such structures. Different focusing regimes can be observed, as well as the increase of focal length with frequency.

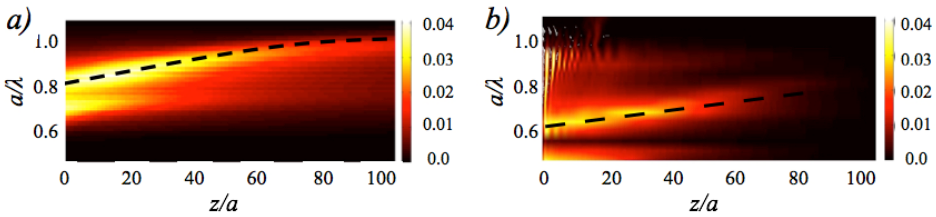

Fig. 4.9 Cross sectional normalized intensity at z=0 plotted against the frequency a/λ for propagation through a rhombic structure along: a) the long diagonal (FBZ edge a/λ=0.85) and b) the short diagonal (FBZ edge a/λ=0.63). The dashed curve indicates the focal point.

4.4. Spatial filtering in MPhC

In the previous sections were dedicated to propagations effects, focalization and self-collimation, directly related to the curvature of the spatial dispersion curves. We now focus our on the spatial filtering performance in MPhCs. The anisotropic losses of such structures allow filtering the noisy components of the incident beam while propagation through a MPhC.

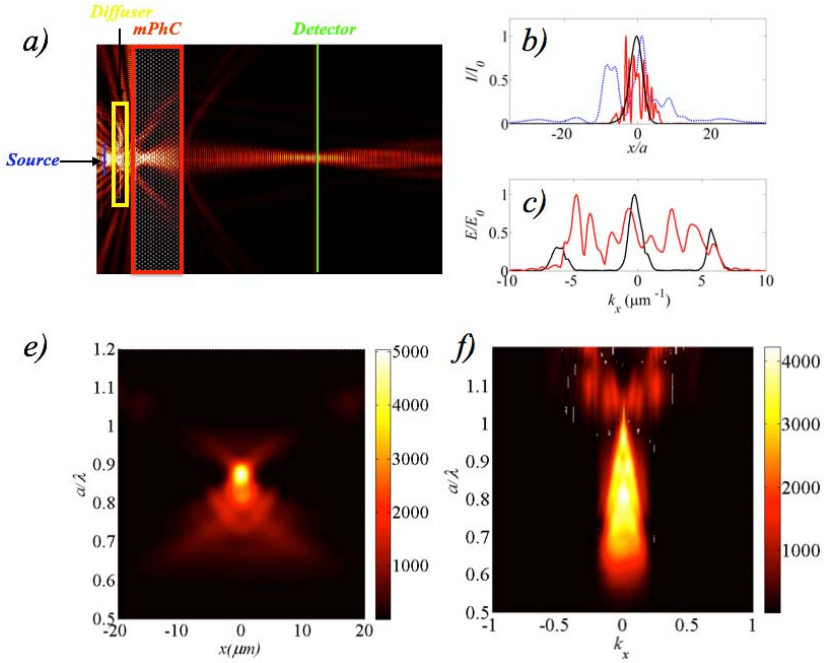

Fig. 4.10. a) FDTD simulation setup used to demonstrate the spatial filtering along the short diagonal of a rhombic MPhCs. A Gaussian source of 3 μm width (blue solid box), passes through a diffuser (yellow box), before crossing the MPhC (thick red box). A detector is placed at the focal point (green thick line). b) Input random beam (red), spatial filtered beam (black) and reference beam propagated in the absence of MPhC (dashed blue). c) FFT profiles of the input beam (red) and spatial filtered beam (black). e)/ f) Intensity map and FFT map at the detector, plotted against the carrier beam frequency in a/λ units.

The spatial filtering shown in Fig. 4.10 is analogous to the previously demonstrated effects in a purely loss modulated media with a similar structural geometry [Kum12].

A diffuser consisting of random radii cylinders generated the random beam from a Gaussian, see Fig. 4.10a. The structure considered is a rhombic geometry with propagation along short diagonal (a_{BZ}=0.83).

Figures 4.10b show the output beam as compared to the noisy input beams, and the same bema propagated through free space. The filtering is also evident comparing the corresponding spectral profiles, as obtained by the Fast Fourier Transform (FFT), see 4.10c, for a carrier frequency of $a/\lambda = 0.76$. Finally, the FFT map of Fig. 4.10f clearly shows that the angular frequency narrows as the frequency increases after $a/\lambda = 0.8$ indicating stronger spatial filtering effect.

Publication V

[Kum 14] N. P. Kumar, L. Maigyte, M. Botey, R. Herrero, and K. Staliunas, *"Beam shaping in two-dimensional metallic photonic crystals",* Journal of the Optical Siciety of America B **31**(4), 686-690 (2014)

ATTENTION ¡
Pages 80 to 84 of the thesis are available at the editor's web
https://www.osapublishing.org/josab/abstract.cfm?uri=josab-31-4-686

Publication VI

[Bot 14] M. Botey, N. P. Kumar, L. Maigyte, R. Herrero, and K. Staliunas, *"Managing spatial diffraction through a periodic loss modulation"*, in SPIE Photonics Europe (pp. 912710-912710). International Society for Optics and Photonics (2014)

ATTENTION ¡
Pages 86 to 92 of the thesis are available at the editor's web
http://spie.org/Publications/Proceedings/Paper/10.1117/12.2051677

Chapter 5

Spatially modulated Broad Area Semiconductors

Chapter index

5.1 Broad Area Semiconductor Amplifiers

One of the possible areas where we expect the concept of (Gain Loss Modulated Material) GLMM to be used to its full potential is Broad emission Area Semiconductor (BAS) lasers and amplifiers, which are important devices for technological applications. Broad Area Semiconductor Amplifiers are capable of emitting at high power with a relatively directional output beam (compared with LEDs). A semiconductor optical amplifier is a forward-biased heavily-doped p^+-n^+ junction fabricated from a direct-bandgap semiconductor material. The main advantage of such lasers is their high conversion efficiency, as the planar configuration enables efficient access of the pump to the whole volume of the active amplifying medium. Therefore, these lasers are widely used in pumping of solid state lasers, free space communication and other applications which requires high electrical-to-optical power conversion efficiency and possibility of choosing spectral characteristics for the intended application [Kru99, Cre14, Naj15, Fri15].

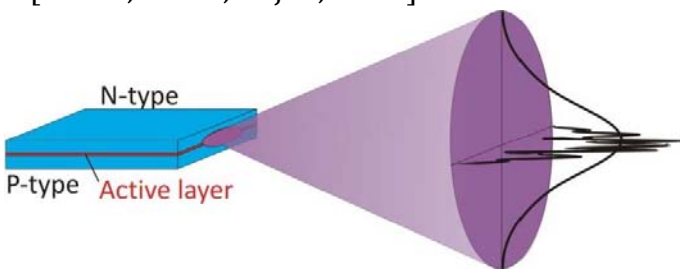

Fig. 5.1 Schematic of a BAS amplifier with fast (vertical) and slow (horizontal) axis.

As shown in the schematic Fig. 5.1, the active layer is sandwiched between p-type and n-type semiconductor layers. The typical size of the active layer is 1 μm × 100 μm. In the vertical (short) direction, the height (e.g. 1 μm) is small enough to obtain single-mode guidance and as a result essentially diffraction-limited beam quality with an M^2 factor only slightly above 1 is obtained. Because of the small aperture size, the beam divergence in this direction is relatively high, with a beam divergence half-angle of 25°. Due to that fast divergence, this is called the *fast axis* direction.

In the long direction (*slow axis* direction), the stripe width may be e.g. 50, 100, 200 μm, or even larger, so that the light is distributed over many spatial modes in this direction. As a result, the beam divergence is much larger than for a diffraction-limited beam with that size, although still significantly smaller than for the fast axis direction. (Typical values are around 5–10° FWHM.). Furthermore, the beam profile may be multi-peaked in the horizontal direction.

The major disadvantages of BAS amplifiers and lasers are a high divergence, which is several times larger than the diffraction limit [Lan91] and an irregular and multi-lobbed output beam [Bur99]. The high divergence in the vertical axis can be easily removed by a cylindrical lens, but if no special mechanisms are incorporated in the design, such as different schemes of optical injection [Gol88, Rad11] or optical feedback [Raa02, Man03] among others, the emission exhibits spatiotemporal fluctuations in the slow axis direction with a broad and noisy angular spectrum. The low spatial quality of the beam can be explained by the lack of an intrinsic mode selection mechanism in the large aspect-ratio cavity of such devices [Bur99, Ada93]. In addition, the Bespalov-Talanov [Bes66] modulation instability in strongly nonlinear regimes leads to filamentation and deteriorates the quality of the emission.

In this chapter, we study the influence of periodically micro-structuring of BAS amplifiers on the spatial quality of the amplified beam. We consider a two-dimensional modulation of the gain function, which can be achieved using a periodical grid of electrodes for the electrically pumped semiconductors, as illustrated in Fig. 5.2a [Kum11]. The periodic modulation of the spatial pump profile, on a spatial scale of several wavelengths, can indeed substantially improve the quality of the amplified beam.

Previous studies show that a periodic gain/loss modulation on a wavelength scale can lead to particular beam propagation effects, such as self-collimation, spatial (angular) filtering, or beam focalization [Sta09, Bot10]. In semiconductor media, due to the linewidth enhancement (Henry) factor, α, a periodical spatial pump distribution causes a combined Gain and refraction Index Modulation (GIM). We note that a very specific and different GIM case is being intensively studied in systems with broken PT-symmetry [Mak08, Lon09]. Here we show that the angular spectrum of the radiation

through a GIM amplifier becomes narrower while being amplified. For sufficiently long propagation distances (of the order of millimeters) we show that the normalized beam quality factor, M^2 [ISO05], can reduce down to unity indicating that the BAS amplifier output becomes perfectly Gaussian for even strongly random initial input beam profiles.

Up to now we considered gain/index modulation profile created by a grid of electrodes for the electrically pumped semiconductors (Fig. 5.2a). However, the gain/index profile can be alternatively created using other techniques as shown in Fig. 5.2: by nonhomogeneous doping of the active layer, modulating the gain layer by ion beam, structuring the material drilling holes on the whole device, modulating the input power by multiple beam interference allowing a temporal control in the structure, or modulating the surface of the semiconductor to generate an effective refractive index grating, among others [Kum11].

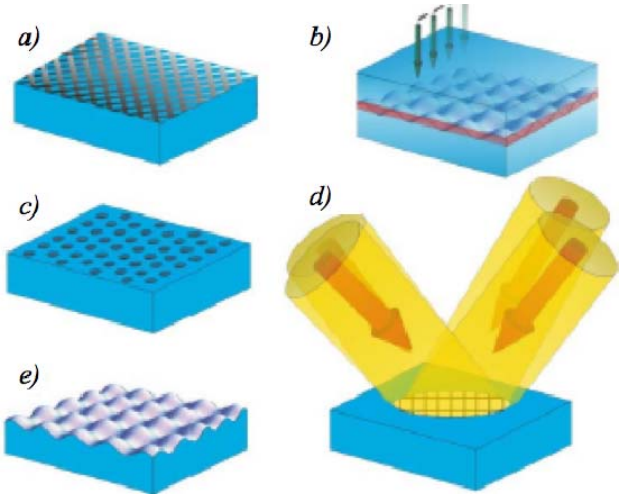

Fig. 5.2 Different schemes to induce a periodic gain/index modulation in Broad area semiconductors , a) structured metallic contact, b) Ion beam structuring of the active layer, c) drilling holes, d) structured optical pumping and e) structuring the surface of the semiconductor.

5.2 Noise reduction in BAS Amplifiers

Many approximations have been considered to model the Broad Band Semiconductor amplifiers and Edge-emitting lasers. For this study we start with the travelling-wave model used in [Agr89, Ult03].

Different models have been derived for this type of devices. A simple mathematical model commonly used for BAS heterostructures with or without current injection can be expressed considering the slowly temporal varying amplitude of field and carrier density [Bram98, Kum11]. A further approximation considers a simple static model consisting of two coupled equations commonly used for modelling BAS heterostructures with and without current injection. The model considers the interaction of the slowly varying amplitude of the field and the carrier density. The electric field is modeled by its amplitude *A* in a paraxial approximation which also includes linear losses and nonlinearities appearing due to the gain and refractive index dependence on the carrier density. An exact treatment of current spreading in the semiconductor active layer would require solving the corresponding 2D Poisson equation, although a simplified approximation is possible [Joy82]. The model consists of two coupled equations for the *TE* polarised electric field (*A*) (Eq.5.1) and the carrier density (*N*) (Eq 5.2):

$$\frac{\partial A}{\partial z} = \frac{i}{2}\frac{\partial^2 A}{\partial x^2} + i\left[-\alpha_h N - i(N-1)\right]A - \gamma A \qquad \text{Eq.(5.1)}$$

$$D\frac{\partial^2 N}{\partial x^2} + p(x,z) - N - BN^2 - CN^3 - (N-1)|A|^2 = 0 \qquad \text{Eq.(5.2)}$$

The rate equation of the carrier density includes radiative and various nonradiative recombination processes that have more or less importance depending on the semiconductor material. The parameter *B* corresponds to the Spontaneous recombination, and *C* takes into account the Auger recombination. The carrier diffusion, *D*, is only taken into account along the transverse direction *x* while diffusion along the propagation direction is neglected because the typical length of carrier modulations is much larger than the diffusion length.

In order to study the spatial evolution of beam profiles along the semiconductor layer, we further simplify the model. First, we neglect the nonradiative recombination terms because they are small in the considered case and have no influence in the qualitative study of beam propagation and the emerging spatial effects.

The pumping profile directly depends on the electrodes structure. However, the carrier diffusion considered in Eq 5.2, always smooths

the profile. Therefore, even in the case of electrodes introducing a stepwise profile, the final effective pump of the active medium approaches a sinusoidal modulation. Neglecting *B* and *C* coefficients and considering smooth enough carrier distributions ($\frac{\partial^2 N}{\partial x^2} << $) and neglecting a small enough diffusion (D<<), we can obtain a first approximation of the carrier distribution: $\overline{N} = \frac{p(x,y) + |A|^2}{1 + |A|^2}$

For small enough diffusion coefficients we can derive an expression for *N* in terms of the modulation function *p(x,z)*, thereby obtaining the expression for the electric field in terms of the modulation function.

$$\frac{\partial A}{\partial z} = \frac{i}{2}\frac{\partial^2 A}{\partial x^2} + \left[\frac{p(x,z)-1}{1+|A|^2}(1-i\alpha) - i\alpha - \gamma\right]A \qquad \text{Eq.(5.3)}$$

where α is the linewidth enhancement factor of the semiconductor and γ is the linear losses which includes scattering losses and cladding layer absorption.

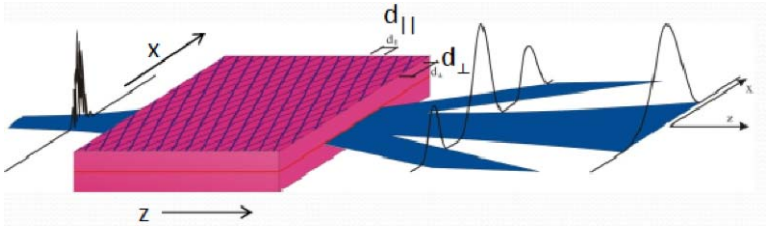

Fig. 5.3 Scheme of a BAS amplifier depicting spatial filtering of a noisy input beam. The periodic modulation of gain profile is obtained by placing periodically arranged metallic contact on the surface substrate material. Lattice constants $d_\perp$ and $d_\parallel$ along x-z direction are shown.

The spatial gain modulation in this BAS amplifiers and lasers scheme is obtained by the spatially distributed pumping rate *p(x,z)*, simultaneously inducing in-phase gain and index modulations due to the α factor. The effective distributed pump can be expressed in terms of geometry as:

$$p(x,z) = p_0 + 4m\cos(q_\perp x)\cos(q_\parallel z) \qquad \text{Eq.(5.4)}$$

where the normalised longitudinal and transverse components of lattice vectors ($q_\perp = \lambda / d_\perp$ and $q_\parallel = \lambda / d_\parallel$) are obtained from lattice

constants $d_{\perp}$ and $d_{\parallel}$ (Fig. 5.3). The adimensional geometry factor can be thus defined as: $Q = 2q_{\parallel}/q_{\perp}^2 = 2d_{\perp}^2/\lambda d_{\parallel}$.
The noise reduction is proved by introducing a noisy beam profile as input. The profile is created by adding multiplicative white noise to a Gaussian beam in the Fourier space :

$$A_{(x,z=0)} = e^{-\frac{x^2}{w_0^2}}(1+\xi(x)) \qquad \text{Eq.(5.5)}$$

where W_0 is the beam width and $\xi(x)$ is the multiplicative white noise with random phase in the frequency space $\varphi(k)$ and constant amplitude a_{noise}, $\xi(k) = a_{noise}e^{-i\varphi(k)}$.

The beam quality is usually defined by the M^2 factor that denotes how small a beam can be focused. It reaches a minimum value of unity for the Gaussian beam. The typical M^2 values for beams emitted by BAS amplifiers are always above 10. This factor is calculated as follows:

$$M^2 = W_0\theta_0\frac{2}{\lambda} \qquad \text{Eq.(5.6)}$$

$$W^2 = 4\frac{\int I(x)\left(x-\rangle x\langle\right)^2 dx}{\int I(x)dx} \qquad \text{Eq.(5.6a)}$$

$$\theta^2 = 4\frac{\int I(k)\left(k-\langle k\rangle\right)^2 dk}{\int I(k)dk} \qquad \text{Eq.(5.6b)}$$

where W_0 is beam waist W at focus and θ_0 is the divergence θ also at focus and they can be calculated integrating the beam intensity in real and frequency space respectively.
The filtering effect can be first studied for a linear regime, i.e. for small field amplitudes. In this case, the field propagation along the crystal is simply:

$$\frac{\partial A}{\partial z} = \frac{i}{2}\frac{\partial^2 A}{\partial x^2} + \left[p(x,z)(1-i\alpha)-(1+\gamma)\right]A \qquad \text{Eq.(5.7)}$$

allowing a simple linear stability analysis to determine the filtering dependence on parameters.

On what follows: Section 5.2.1 describes the beam quality improvement for BAS amplifiers without linewidth enhancement factor while Section 5.2.2 describes the same considering the typical linewidth enhancement factor of these semiconductor materials.

5.2.1 BAS with linewidth enhancement factor $\alpha \approx 0$

The linewidth enhancement factor α (Henry factor) is defined as the ratio of imaginary and real part of the induced complex refractive index (m_i/m_r). For a material with $\alpha \approx 0$, the gain is introduced by the electric pump while the refractive index remains unchanged or with very small variations that can be neglected. In the case of a structured pump, these materials would only exhibit spatial gain-loss modulations and the effective complex refractive index of the material would only show real part $m = m_r$. Thus, BAS amplifiers with $\alpha \approx 0$ present similar results to the ones shown by LMM materials described in Chapter 3, and in particular, it is expected that such materials show flat lensing and spatial filtering effects around the resonance point (here $Q = 1$).

The linearity of the system for small enough field amplitudes allows a semi-analytically treatment to obtain the spatial dispersion relations. Parameters are tuned near the resonance to reproduce the filtering effect, already described in Chapter 3 complemented by a focusing effect associated to the particular diffraction of the most amplified mode inside the crystal.

To visualize the filtering performance of the structure a noisy Gaussian beam is propagated through the modulated medium. The beam experiences the typical diffusive square root broadening with distance. The filtered beam at the output is focalized beyond the crystal due to the negative phase shift accumulated in propagation, see Fig. 5.4a. Intensity profiles measured at the focal plane shows the spatially filtered output beam, as shown in Fig. 5.4b.

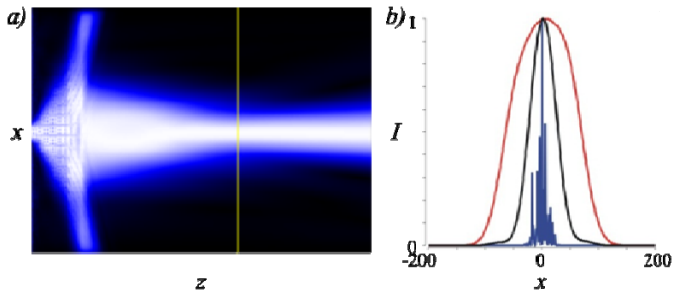

Fig. 5.4 a) Spatial filtering effect demonstrated in gain modulated BAS with complex refractive index m = 0.1 and $Q_{//}$ = 0.85. b) Input random beam (blue), output beam exiting the crystal (red) and beam profile at the focal plane (black).

The geometry factor is scanned around the resonance point Q=1 to see the effects on diffraction and spatial filtering (Fig. 5.5).
Analogously to the results observed for LMM [Kum13, Kum14], Section 3.2, a region of negative diffraction inside the crystal for $Q < 1$ is obtained and flat lensing is achieved. The corresponding positive focal distance can be seen in Fig. 5.5a. At the other side of resonance, $Q > 1$, the beam has a normal diffraction inside the crystal and the focal length becomes negative. The sign changes in the curvature of the crystal dispersion has been already explained using mode coupling arguments in Section 3.2.1. It can also be seen that near resonance (Q = 1), where the strongest anisotropy of the gain is leading the beam propagation and the spatial filtering effect becomes maximal, M^2 values approach unity and the beam amplification reaches the highest values (Fig. 5.5b). Larger crystal lengths create wider filtering windows always centred at resonance. Figure 5.5 also demonstrates the small dependence of the filtering effect on the noise amplitude. This is well understood considering that the filtering effect is based on the anisotropic gain. It is also remarkable the small number of necessary periods to obtain the filtering.

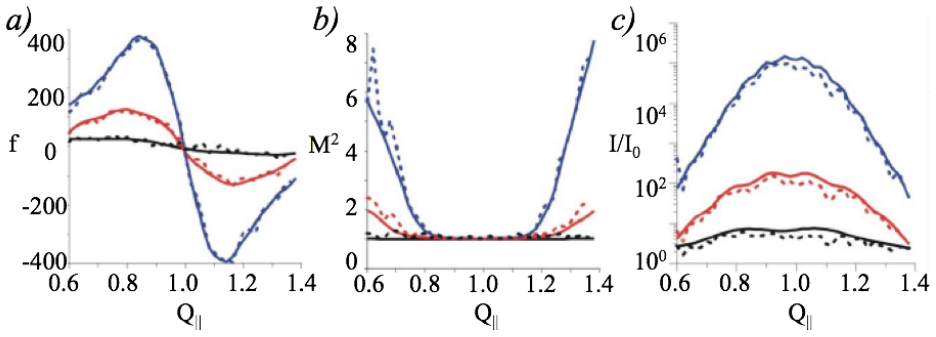

Fig. 5.5 Variation of a) focal length b) M^2 and c) intensity at the focal point (in terms of the input intensity I_0) as a function of the geometry factor Q for a BAS with linewidth enhancement factor $\alpha \approx 0$. Solid (dashed) lines correspond to noise amplitudes of $a_0 = 0$ ($a_0 = 1$). Black, red and blue colours correspond to crystal lengths of $2d_{//}$, $4d_{//}$, $8d_{//}$ respectively.

5.2.2 BAS amplifiers with linewidth enhancement factor $\alpha \neq 0$

Generally BAS amplifiers will have a nonzero linewidth enhancement with values of $3<\alpha<8$ simultaneously appearing gain and index modulation in the semiconductor structure. It provides anisotropic gain profiles giving to the semiconductor the ability to spatial filter the beam propagating through. Moreover, the diffraction management is also feasible, obtaining negative diffraction and non-diffractive propagation of the beam along the crystal. This kind of complex refractive index modulations and the associated effects are observed in metallic photonic crystals and have been explained in Chapter 4. There, a deeper study has been carried out using FDTD simulations in metallic PhCs to prove these effects [Kum13].

Here, we consider a typical $\alpha = 3$ scenario to compute the beam propagation properties in BAS amplifier. The complex refractive index then becomes $0.03+0.09i$. Propagation along a BAS amplifier is shown in Fig. 5.6. The main difference with the $\alpha = 0$ case is the non-degenerated diffraction for the amplified and depleted mode (Fig. 5.6c).

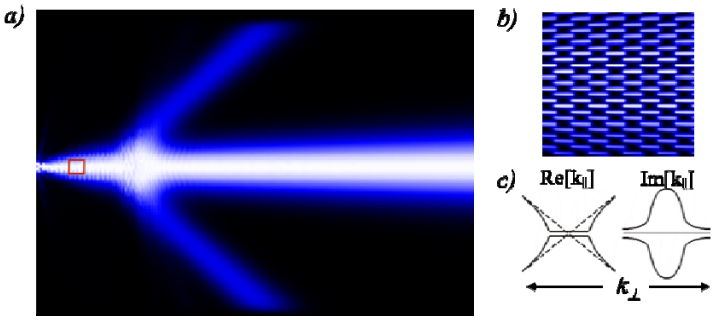

Fig. 5.6 Beam propagation in a BAS. The inset b) shows the most amplified mode. c) Real and imaginary part of dispersion. The dashed lines in the real part show the dispersion in homogenous media.

In this case, the output beam diverges and the focalisation behind the crystal is not seen, so in order to measure the M^2 value, we propagate the beam in backward direction and find the virtual focal point.

The focal length depends on the structural geometry as shown in Fig. 5.7a, for a Gaussian beam with $a_0 = 1$. The red and black curve represents propagation in a longer crystal with 16 periods and shorter crystal with 4 periods respectively. It was seen that, the focal length of the beam exiting the crystal is always negative, implying that the beam is diverging in most of cases. Scanning the geometry factor Q a regime of spatial filtering is observed just after resonance, $Q>1$ (Fig. 5.8b). It can be seen that the beam quality factor M^2 approaches 1 with a minimum value of 1.006 for a longer crystal while for the shorter crystal the minimum value is 1.15.

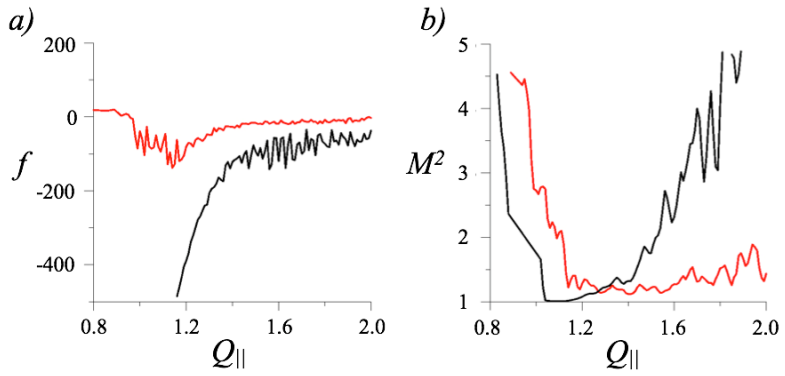

Fig. 5.7 a) Dependence of the focal distance (a) and beam quality factor (b) on geometry factor Q for a short ($L = 4d_{||}$) (in red) and a long ($L = 16d_{||}$) (in black).

In the longer crystal case the M^2 values approaching unity even for larger noise amplitudes introduced in the input beam seems to point out that for long enough crystal lengths, the output profile is strongly related to the anisotropic gain and has almost no dependence on the input beam. The different transverse modes with small wavenumber are exponentially amplified along propagation with different strength while transverse modes associated to noise and with large wavenumbers are not amplified.

We finally note that this the presented study is a preliminary study limited to small field amplitudes and the considered BAS model has been reduced to only one field equation.

Publication VII

R. Herrero, M. Botey, N. Kumar, K. Staliunas, "Dispersion management in spatially modulated broad band semiconductors", 13th International Conference on Transparent Optical Networks. Institute of Electrical and Electronics Engineers (IEEE), (2011)

Publication VIII

R. Herrero, M. Botey, N. P. Kumar, and K. Staliunas, *"Spatial noise reduction in broad area semiconductors"*, 13th International Conference on Transparent Optical Networks. Institute of Electrical and Electronics Engineers (IEEE) (2012)

Publication IX

R. Herrero, M. Botey, N. P. Kumar, and K. Staliunas, *"Improving beam quality in broad area semiconductor amplifiers",* SPIE Photonics Europe. International Society for Optics and Photonics,(2012)

Improving beam quality in broad area semiconductor amplifiers

Ramon Herrero[1], Muriel Botey[3], Nikhil P.Kumar[1], Kestutis Staliunas[2]
[1]*Departament de Física i Enginyeria Nuclear, Universitat Politècnica de Catalunya, Colom 1, 08222 Terrassa, Spain*
[2]*Institució Catalana de Recerca i Estudis Avançats (ICREA), Departament de Física i Enginyeria Nuclear, Universitat Politècnica de Catalunya, Pg. Ernest Lluch / Rambla Sant Nebridi, 08222 Terrassa, Spain*
[3]*Departament de Física i Enginyeria Nuclear, Universitat Politècnica de Catalunya, Comte Urgell 187, E-08036 Barcelona, Spain*
e-mail: ramon.herrero@upc.edu

ABSTRACT

Broad area semiconductors lasers and amplifiers are of technological relevance because of their high conversion efficiency and high output power, in a wide range of wavelengths. However, due to their specific waveguiding planar geometry, which is unique to this kind of heterostructures, the beam is usually of low spatial and temporal quality. Therefore, the beam quality restricts their potential use. We propose to improve the beam quality semiconductors lasers and amplifiers using a two-dimensional spatial modulation of both the refractive index and the optical gain/loss, on the order of the wavelength. The modulation of the refractive index modifies the spatial dispersion, allowing the possibility to manage diffraction. Besides, the gain/loss modulation introduces anisotropic gain and the possibility to manage diffusion. As a result, the modified dispersion gives rise to interesting and technologically useful effects, such as spatial filtering or focalization behind the material. We show that such effects can be achieved considering a modulated injection current which imposes a periodic spatial modulation to the active layer of the semiconductor.

Keywords: broad emission area semiconductor laser, photonic crystals, gain-loss modulation;

1. INTRODUCTION

Propagation of light in structured materials has been very extensively studied in the last decade[1-3]. In the well known case of Photonic Crystals (PhC), where the refractive index is modulated on a wavelength scale, the modification of the spatial dispersion curves allows the management of effective diffraction. Effects such as self-collimation and negative diffraction are based upon this phenomenon[4-9]. Self-collimation effects were also predicted and observed in acoustics [10, 11]. Similar materials, where the gain/loss is modulated on the wavelength scale, known as Gain/Loss Modulated Materials (GLMMs), have just been recently studied showing other important spatial beam propagation effects [12, 13]. While an angular dependence on phase and group velocity appears both in PhCs as well as in GLMMs, in the later case also an angular dependence of the wave amplification/attenuation arises. Such gain/loss anisotropy can be used for applications such as beam spatial filtering. The directional gain is attributed to the appearance of sharp peaks in the imaginary part of the eigenfrequencies, which corresponds to an anisotropic gain in k-space (in angular domain), arising from gain/loss modulation on a small spatial scale. We note that spatial filtering has also been proposed for PhCs[14]; however the first experimental evidences showed a relatively weak effect[15].

First studies involving two dimensional (2D) GLMM were performed using a paraxial model, in which different beam shaping effects such as self collimation, superdiffusion, focalization behind the crystal and high directivity of gain were shown[12]. A subsequent study, based on a plane wave expansion method, predicted the distortion of the spatial dispersion in both the real and the imaginary eigenfrequency components[13]. In a more recent study, the angular transmission response of a material with modulated loss was calculated and numerically proven using finite a difference time domain method[16].

One of the possible areas where we expect the concept of GLMM to be used to its full potential is Broad emission Area Semiconductor (BAS) lasers and amplifiers, which are important devices for technological applications. As amplifiers or lasers, they are utile in many applications due to their high power output, as e.g. to pump solid state lasers. BAS lasers are efficient light sources since their geometry allows an efficient access to pump to the entire material. On the other hand, the emitted radiation is usually strongly divergent due to the fact that many spatial modes are excited and involved in the emitted beam. Additionally, in broad-area gain regions light can spread because of the lack of any lateral confinement. This allows local self-focusing effects due to local increments of refractive index or local amplifications of field intensity. Light dynamics in such lasers has been widely studied due to its interesting characteristics[17-19].

In fact, not only spatial patterns related to the simultaneous emission of many transverse modes, but also a complicated spatio-temporal dynamics is observed, which involves the presence of several longitudinal mode families. All these effects cause beam instabilities and filamentation which can easily take place in these devices, drastically decreasing the emitted output beam quality[20, 21]. Thus, applications of such devices are mainly restricted to situations that do not require high beam quality.

In this work we consider a monochromatic beam passing through a BAS amplifier with a spatial modulation in both transversal and longitudinal directions. Different schemes can be considered to impose the spatial modulation. Here the modulation is imprinted by a spatially modulated pump through a modulated current injection using grid-like electrodes. In semiconductor materials, the effective gain depends on the injection current across the amplifying layer. Additionally, the current induces a refractive index variation, and both, the gain and index variations are related by the so called linewidth enhancement factor (α).

2. MODEL AND SETUP

Different mathematical models have been developed for BAS lasers and amplifiers. Here we consider a simple static model consisting of two coupled equations which is commonly used for BAS heterostructures with or without current injection. The model considers the interaction of the slowly varying amplitude of field E and carrier density N [22,23]. The electric field is modeled by its amplitude A in a paraxial approximation which also includes linear losses, η, and nonlinearities appearing due to the gain and refractive index dependence on the carrier density, which is considered to be linear in the model. The rate equation of the carrier density includes diffusion D, and spontaneous, B, and Auger, C, recombination coefficients. The model can be written in terms of normalized variables (keeping the usual notation [24]):

$$\frac{\partial A}{\partial z} = i\frac{\partial^2 A(x,z)}{\partial x^2} + \left[(1-i\alpha)N - (1+\eta)\right]A(x,z), \tag{1}$$

$$D\frac{\partial^2 N}{\partial x^2} + p(x,z) - N - BN^2 - CN^3 - (N-1)|A|^2 = 0, \tag{2}$$

where $p(x,z)$ is the normalized pumping rate which is considered to be of a sinusoidal form

$$p(x,z) = p_0 + 4m\cos(q_x x)\cos(q_z z). \tag{3}$$

In the following, the recombination terms are neglected in the carrier rate equation (B=C=0). The carrier diffusion smooths the spatial variations of the carrier density. It results in a decrease in amplitude of a sinusoidal modulation and it is not considered here for simplicity (D=0). With this approximations and considering small electric field amplitudes, the normalized carrier density is given by the pumping rate $N(x,y) = p(x,z)$ and the model is thereby reduced to the field equation:

$$\frac{\partial A}{\partial z} = i\frac{\partial^2 A}{\partial x^2} + \left[(1-i\alpha)p - (1+\eta)\right]A \tag{4}$$

The constant part $(1+\eta)A$, irrelevant for the spatial effects since it only introduces an exponential gain or loss, will not be considered in the following simulations.

The studied setup consists on a semiconductor structure of 0.28mm width and 2.5 mm length. The modulation period in the propagation direction z varies around 200 μm and is fixed to 8.9 μm in the transverse direction x. The amplitude of the gain modulation is 3980 m^{-1} obtained by a nonhomogeneous injection current and the enhancement factor of the semiconductor has a typical value of $\alpha = 3$ that corresponds to a refractive index amplitude of 9.5 10^{-4}. The structure is calculated for a wavelength λ=0.5mm and the input beams are considered to propagate along the long diagonal of the structure (in the z direction).

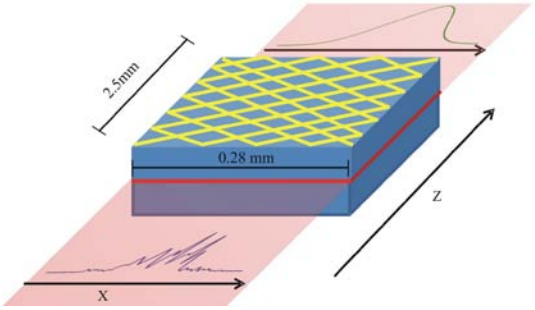

Figure.1. BAS amplifier with grid-like electrodes. The non-homogeneous injection current generates a spatial modulation of gain and refractive index in the active layer of the semiconductor. A noisy beam injected at the entrance, is spatially filtered at the output.

2.1 Linear analysis

The problem can be analytically treated performing a harmonic expansion of the field, and just considering the three most relevant harmonics with periodicities of the gain/loss modulation.

$$A(x,z) = \exp(ik_x x)\cdot\left[a_0 + a_{-1}\exp(-iq_x x - iq_z z) + a_1 \exp(+iq_x x - iq_z z)\right] \tag{5}$$

Introducing eq. (5) is in eq. (4), we obtain the evolution of the three harmonics:

$$da_0/dz = \left(-ik_\perp^2/2 + g\right)a_0 + (1-ih)m(a_1 + a_{-1}) \tag{6.a}$$

$$da_{\pm 1}/dz = \left(-i(k_\perp \pm q_\perp)^2/2 + iq_\parallel + g\right)a_{-1} + (1-ih)ma_0 \tag{6.b}$$

The constant complex gain $g = p_0\,(1\text{-}h)\,\text{-}1\,\text{-}\alpha$ is irrelevant for the study of spatial propagation effects, and can be eliminated from eq.(5) by considering an exponentially growing/decaying field. Next, we perform a standard analysis looking for the exponentially growing eigenmodes: $a_0, a_{-1}, a_1 \propto \exp(ik_z z)$, where the exponential growth is incorporated into the imaginary part of k_z. This is essentially a linear stability analysis analogous to that performed for the pure GLM case[13] and for the case of photonic crystals[8]. The analytic expressions for the propagation exponents are cumbersome; therefore the calculations are performed numerically.

Eigenmodes with positive imaginary part of k_z are amplified along propagation while negative ones are decaying. Thus, the beam shape behind the crystal is directly related with the branch of eigenmodes with the largest imaginary k_z component. Fig.2 shows the eigenvalues for the parameters used. The angular dependence of the amplification (the imaginary part of k_z) can act as a spatial low-pass filter and can eliminate the undesirable noise from the beam.

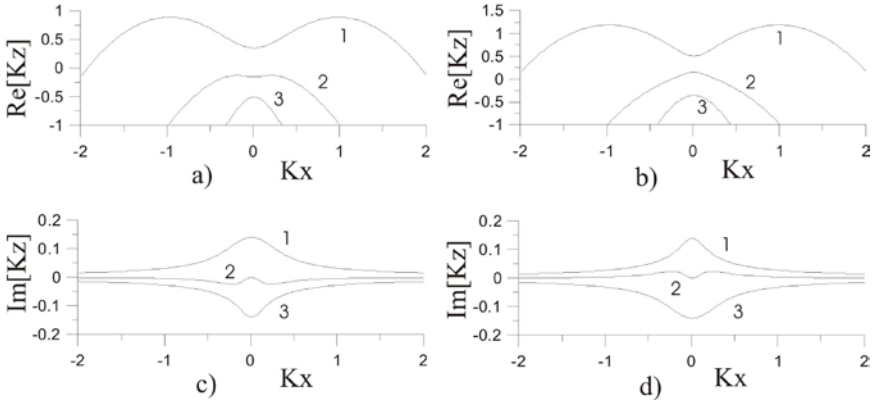

Figure.2: a),b) Real and c),d) imaginary parts of eigenvalues for $Q_{||}$=0.85 (a,c) and $Q_{||}$=1.15 b),d). The negative and positive curvature of the curves in a),b) correspond to positive and negative diffraction regimes, and the flattening denotes self-collimation. c),d) show the angular profile of the eigenmodes which correspond to the field amplification.

The eigenvalues describe the beam evolution along the crystal in a qualitative way. The real part of eigenvalues is related to the phase curvature accumulated during propagation, while the imaginary part corresponds to the amplification of the field. There are main differences to be notes between eigenvalues for the two $Q_{||}$ values considered in Fig. 2. On one hand, it can be seen from the imaginary part (fig.2 c,d) that two eigenmodes are amplified in $Q_{||}$=1.15 case, while only one mode is amplified for $Q_{||}$=0.85; and this mode presents a wider lobe than the most amplified mode of $Q_{||}$=1.15. Secondly, analyzing the real part (fig.2a,b), the most amplified mode of both cases presents a positive second derivative for small $|k_x|$ values that corresponds to a negative diffraction of light in propagation. The main difference for this real part is the stronger curvature observed for the $Q_{||}$=1.15 case. The second amplified mode that appears for $Q_{||}$=1.15 presents a negative second derivative for small $|k_x|$ values that corresponds to a large positive diffraction.

3. FILTERING

Numerical calculations were performed in a simplified model, without linear absorption and carrier diffusion. The input beam is considered to be a monochromatic Gaussian beam with λ = 0.5μm and 14μm width, focalized at the entrance of the active media and propagating along the long diagonal (*z* direction). The input beam noisy profile is built by addition of multiplicative white noise, ξ.

$$I_{input}\ x\ = I_0 e^{-(x/W_0)^2}\left(1+0.5\xi\right) \tag{7}$$

A pseudospectral split-step method is used. The transverse space is discretized on a grid of 512 points. Fig.3 shows the integration of the beam along *z* direction inside the modulated semiconductor material and along the distance of 12.5 mm behind it, in free space. The beam broadening inside the material presents a square root dependence on the propagated distance that is characteristic of diffusive broadening (Fig.2 a,c). The spatial modulation observed inside the material indicates that the propagated beam is in fact the envelope of the amplified eigenmode.

The negative diffraction obtained with these semiconductor parameters for small k_x values (Fig.2.a), results in the beam focalization at some distance behind the material. The two sidebands correspond to large k_x values that diverge rapidly behind the crystal. The energy distribution among the central mode and sidebands at the crystal output is very similar to GLMM materials: the energy in the central beam is approximately 50% of the total energy.

The narrower gain lobe for $Q_{||}$=1.15 corresponds to stronger diffusion of light inside the crystal (fig.2d). Negative diffraction of amplified modes inside the crystal accumulates a negative curvature in the wave-front that focalizes the output beam for both cases. The larger curvature in the dispersion curve observed for the $Q_{||}$=1.15 amplified mode corresponds to a larger focalization distance (fig.3).The $Q_{||}$=1.15 case presents a positive and a negative curvature for the

two amplified eigenmodes, respectively. However, the output beam is mainly composed by the most amplified eigenmodes, with negative diffraction inside the crystal. For $Q_{||}$=1.15 nearly the 64% of energy goes to the central beam while for $Q_{||}$=0.85 this value is reduced to the 40%.

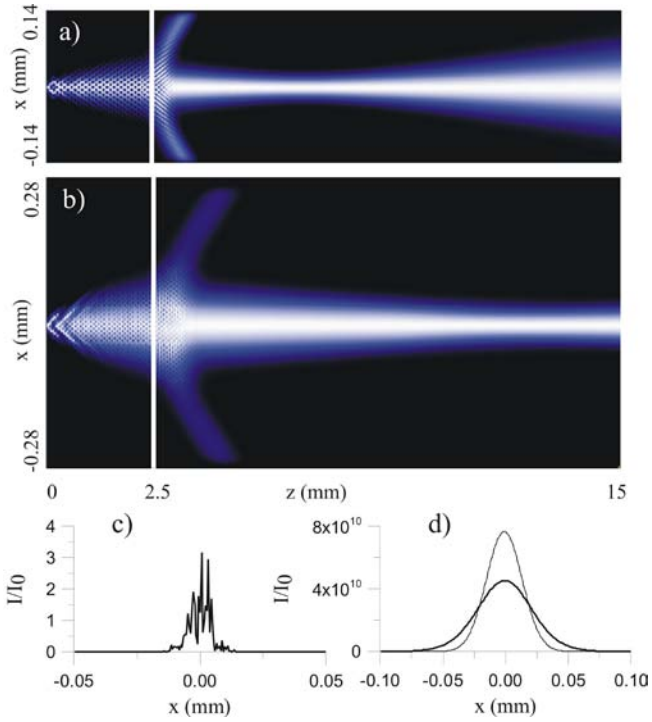

Figure.3. Propagation of an incident Gaussian beam through the semiconductor 2D active layer for a) $Q_{||}$=0.85, b) $Q_{||}$=1.15. c) Noisy incident beam d) beam at the focal where the width reaches a minimum value for $Q_{||}$=0.85 (thin line) b) $Q_{||}$=1.15 (thick line).

In order to quantify the evolution of beam quality, we calculate the normalized beam width $\overline{W}$, given by the beam width W and the beam divergence θ

$$\overline{W} = \frac{2}{\lambda} W\theta\,, \quad \frac{W^2}{2} = \frac{\int I(x)(x-<x>)^2\,dx}{\int I(x)dx}\,, \quad \frac{\theta^2}{2} = \frac{\int I(k)(k-<k>)^2\,dk}{\int I(k)dk} \tag{8}$$

At the focus of the beam, the normalized beam width is called M^2. The value of this factor is unity for a Gaussian beam at focus (flat wave front) and increases with the spatial modulation of the beam envelope.

The value of $\overline{W}$ for a noisy input beam is about 10, denoting a profile with large spatial noise (the spectrum is broadened $\approx$ 10 times due to the noise). $\overline{W}$ increases along the crystal in an oscillating way and, just behind the crystal, acquires large artificial values due to the diverging sidebands that are absorbed at the boundaries (Fig.3a). The central beam focalizes due to the negative curvature acquired inside the crystal, because of its negative diffraction. The $\overline{W}$ value of the amplified and filtered beam reduces to values about 1.0 at the focal point. The lowest value found in the simulation is 1.000777.

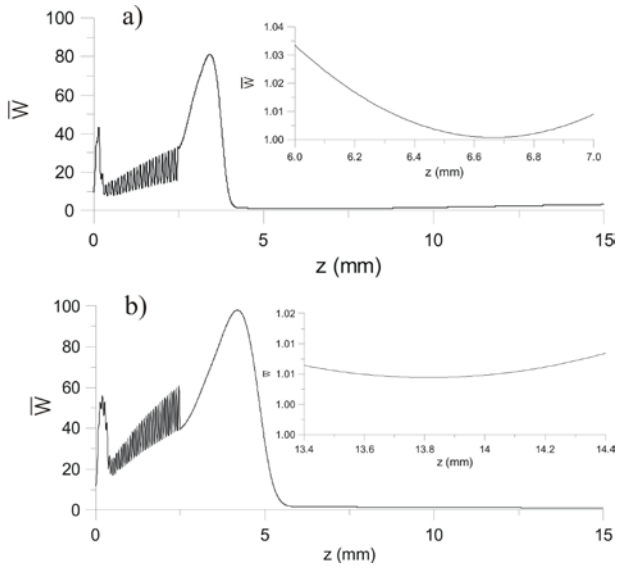

Figure.4 Evolution of $\overline{W}$ along the propagated direction for $Q_{||}$=0.85 and $Q_{||}$=1.15. The inset shows a zoom in plot near the focal point where $\overline{W}$ reaches the minimum value. In both cases M^2 value approaches 1.

4. CONCLUSIONS

We considered a simplified model to numerically simulate a BAS amplifier with a spatially modulated injection current. Such injection current introduces both a gain and a refractive index modulation in the material which amplitudes are linked by the so called α-factor of the semiconductor. In this way, the active 2D slice can be considered as a 2D gain/loss modulated material also exhibiting an index modulation on the wavelength scale. Our model considers an incident beam that propagating in-palne inside the active semiconductor slab, and along the largest diagonal of the rhombic structure. Integration is performed using paraxial approximation.

Numerical results evidence filtering effects in a Gaussian beam with multiplicative white noise. The quantification of the beam improvement is estimated by means of the M^2 coefficient which gives the relative distance between the evaluated profile and a perfect Gaussian beam. The M^2 value of the amplified beam approaches 1, meaning that all noise is filtered out.

ACKNOWLEDGEMENTS

The work was financially supported by Spanish Ministerio de Educación y Ciencia and European Union FEDER through project FIS2008-06024-C03-02 and FIS2011-29731-C02-01.

REFERENCES

[1] E. Yablonovitch, “Inhibited Spontaneous Emission in Solid-State Physics and Electronics,” Phys. Rev. Lett. 58, 2059–2062 (1987).
[2] S. John, “Strong localization of photons in certain disordered dielectric superlattices,” Phys. Rev. Lett. 58, 2486-2489 (1987).
[3] J. D. Joannopoulos, R. D. Meade, and J. N. Winn, “Photonic Crystals: Molding the Flow of Light,” Princeton University Press, Princeton, 1995.
[4] R. Zengerle, “Light propagation in singly and doubly periodic planar waveguides," J. Mod. Opt. 34, 1589–1617 (1987).

[5] H. Kosaka, T. Kawashima, A. Tomita, M. Notomi, T. Tamamura, T. Sato, S. Kawakami., "Self-collimating phenomena in photonic crystals," Appl. Phys. Lett. 74, 1212-1214 (1999).
[6] Peter T. Rakich, Marcus S. Dahlem, Sheila Tandon, Mihai Ibanescu, Marin Soljai, Gale S. Petrich, John D. Joannopoulos, Leslie A. Kolodziejski & Erich P. Ippen, "Achieving centimetre-scale supercollimation in a large-area two-dimensional photonic crystal," Nat. Mater. 5, 93-96 (2006).
[7] T. Pertsch, T. Zentgraf, U. Peschel, A. Brauer, and F. Lederer," Anomalous Refraction and Diffraction in Discrete Optical System," Phys. Rev. Lett. 88, 093901 (2002).
[8] K. Staliunas and R. Herrero, "Nondiffractive propagation of light in photonic crystals," Phys. Rev. E 73, 016601 (2006).
[9] Yurii Loiko, Carles Serrat, Ramon Herrero, Kestutis Staliunas, "Quantitative analysis of subdiffractive lightpropagation in photonic crystals," Opt.Comm., 269, 128-136 (2007).
[10] I. Pérez-Arjona, F. Redondo, V. J. Sánchez-Morcillo, V. Espinosa, and K. Staliunas, "Theoretical prediction of the nondiffractive propagation of sonic waves through periodic acoustic media," Phys. Rev. B 75, 014304 (2007).
[11] V.Espinosa, V. J. Sanchez-Morcillo, K. Staliunas, I. Perez-Arjona, J. Redondo, "Subdiffractive propagation of ultrasound in sonic crystals," Phys. Rev. B 76, 140302(R) (2007).
[12] K. Staliunas, R. Herrero, R. Vilaseca, "Subdiffraction and spatial filtering due to periodic spatial modulation of the gain-loss profile," Phys. Rrev. A 80, 013821 (2009).
[13] M. Botey, R. Herrero, K. Staliunas, "Light in materials with periodic gain-loss modulation on a wavelength scale," Phys. Rev. A 82, 013828 (2010).
[14] K. Staliunas and V. J. Sánchez-Morcillo, "Spatial filtering of light by chirped photonic crystals," Phys. Rev. A 79, 053807 (2009).
[15] L. Maigyte, T. Gertus, M. Peckus, J. Trull, C. Cojocaru, V. Sirutkaitis, and K. Staliunas, "Signatures of light-beam spatial filtering in a three-dimensional photonic crystal," Phys. Rev. A 82, 043819 (2010).
[16] N. Kumar, M. Botey, R. Herrero, Yu. Loiko, and K. Staliunas, "High directional gain in periodic Gain/Loss modulated materials,"submitted to Phot. Nano. Fund. Appl. 2012.
[17] M. Zymanski, "Theoretical analysis of broad-area semiconductor lasers with laterally shifted modal reflectors," Optical and Quantum Electronics 35, 147–160 (2003).
[18] H. Adachihara, O. Hess, E. Abraham, P. Ru, and J. V. Moloney, "Spatiotemporal chaos in broad-area semiconductor lasers," J. Opt. Soc.Amer. B, vol. 10, 658–665 (1993).
[19] T. Burkhard, M. O. Ziegler, I. Fischer, and W. Elsäßer, "Spatio-temporal dynamics of broad area semiconductor lasers and its characterization," Chaos Solitons Fractals, vol. 10, 845–850 (1999).
[20] O. Hess, T. Khun, "Spatio-temporal dynamics of semiconductor lasers: Theory, modelling and analysis," Prop. Quant. Eectr. 20, 85-179 (1996).
[21] O. Hess, S. W. Koch, and J. V. Moloney, "Filamentation and beam propagation in broad-area semiconductor lasers," IEEE J. Quantum Electron., vol. 31, 35 - 43 (1995).
[22] Balsamo S, Sartori F, Montrosset I, "Dynamic beam propagation method for flared semiconductor power amplifiers," IEEE J. Sel. Top. Quantum Electron. 2(2), 378–384 (1996).
[23] A. Egan, C. Z. Ning, J. V. Moloney, R. A. Indik, M. W. Wright, D. J. Bossert, and J. G. McInerney, "Dynamic instabilities in master oscillator power amplifier semiconductor lasers," IEEE. J. Quantum. Electron. 34(1), 166–170 (1998).
[24] E. A Ultanir, D. Michaelis, F. Lederer, G. I. Stegeman, "Stable spatial solitons in semiconductor optical amplifiers," Opt. Lett. 28, 251-253 (2003).

Chapter 6

Conclusions

In this last chapter I summarize the main results or achievements obtained during my PhD. Besides, I will also briefly report on some other works that appeared later or sometimes almost overlapping my results, some of which represent direct extensions of results here presented, other may be even regarded as a continuation in the field, for which the results of this PhD could have been inspiring.

My first study [Kum12, Bot11], presented in Chapter 3, provides our initial results on beam propagation in Loss-Modulated Media (LMM), as a particular case representative of Gain Loss Modulated Media (GLMM), where, ideally, only losses are considered to be modulated on the wavelength scale. In this way, we provide the first numerical confirmation on previous analytical predictions for GLMMs. We numerically prove, by means of the FDTD method, the highly angular gain/loss response of LMM structures. The result represents a confirmation of the predictions performed under paraxial approximation of ref. [Sta09]. Close to the edges of the First Brillouin Zone (FBZ) of a LMM, a narrowing of the spatial spectrum is observed. This effect can be related to the coupling and locking of spatial harmonic components propagating along ΓM direction. Besides, it is demonstrated that such strong anisotropy of losses can be used for spatial filtering purposes. We precisely show the effect by filtering out the high angular components from the transverse profile of a noisy beam in relatively short propagation through the LMM. Although angular narrowing of the gain profile is found for both square and rhombic geometries, the spatial filtering results to be slightly more pronounced for a rhombic geometry and for light beams propagating along the long diagonal of the structure. The demonstrated filtering effect of LMM structures could be used, for instance, to amplify and filter out, by means of optical methods, the information signals from the noisy background in optical communication systems, either fiber based or free space. Compared to conventional mechanisms, the main advantage of the spatial proposed filtering method is that it requires an extremely short propagation distance and, therefore, it could be directly integrated in micro-optical systems.

The second milestone of my phD, is the study of the effect of LMM materials on the diffractive properties of light beams. The results presented in [Kum13, Bot13] show that LMM materials with periodic modulations on the wavelength scale can lead to substantial focalization of a beam propagating through a short slab with flat–flat

interfaces, confirming the result also hinted in ref. [Sta09]. In the study we consider three different structural geometries, corresponding to propagation along the diagonals of a rhombic and square lattice, and, in all cases, we find analogous results. The light intensity map of a Gaussian beam exiting the structure exhibits a high-transmission window for frequencies close to the edges of the FBZ, which results from the anisotropic attenuation provided by the periodicity. For LMM, such high transmittance occurs precisely at frequencies where a low transmission or photonic bandgap opens in the case of Photonic Crystals (PhCs). The focusing after the crystal slab with a thickness of ten wavelengths is confirmed by a deeper analysis of the phase profile. For given frequencies, the phase curvature becomes positive, indicating negative diffraction, which provides focalization beyond the structure. Moreover, the numerically obtained curvature follows the analytical estimations based on the second derivative of the spatial dispersion diagrams. The control of light beam propagation by miniaturized devices is important not only from a fundamental point of view but also as an actual requirement for applications. The predicted phenomenon is expected to be generic for spatially modulated materials and other kinds of waves, such as, for instance, acoustic waves in lossy sonic crystals. Indeed, we also discuss for the first time, the effect of loss modulations in acoustic crystals. Angular transmission bands were also predicted in acoustic LMM crystals.

The results reported in refs. [Kum14, Bot14], Chapter 4, represent a more realistic scenario: beam propagation is investigated in an actual LMM. We investigate beam-shaping effects in 2D rhombic metallo-dilectric crystals, made of gold cylinders embedded in air. For given frequencies, a clear focalization of the beams behind a thin flat Metallic PhC (MPhC) slab is observed. It is shown that the focalization is due to negative diffraction propagation inside the crystals, accounted by convex spatial segments on the spatial dispersion, and then compensated in free space up to focus. Moreover, we prove another important unknown result: that the dependence of the focal position on frequency is clearly explained by the curvature of the spatial dispersion segments. Additionally, nondiffractive propagation through the structure is demonstrated; the spatial shape of the beams is kept constant with propagation within the structure, in this case, at frequencies for which the spatial dispersion curve exhibits flat segments. Finally, we investigate the spatial filtering performance within this same structure. We show that high spatial Fourier harmonics of a noisy beam are removed by

propagation through the MPhC, leading to an improvement of its spatial quality. The focusing performance of narrower beams is weaker than for broader ones. While the drawbacks of metal structures are losses, as part of light is absorbed, we point out that they provide new perspectives in light manipulation on the micrometer scale. MPhCs are miniaturized devices that give spatial control over beam propagation, and their study may be important from the fundamental point of view as well as for applications.

As another possible direct application of the previous idea, we present some initial investigations in the conference proceedings [Her11, Her12, Her12-2], on how spatially cleaning of beams can be achieved in Broad Area Semiconductor Amplifiers using the previous ideas, that is to say, introducing an intrinsic filtering mechanism by modulating the gain/loss of the active material. We considered a simplified model reduced to only one field equation, to numerically simulate a BAS amplifier with a spatially modulated injection current. Such injection current introduces both a gain and a refractive index modulation in the material which amplitudes are linked by the so-called α-factor of the semiconductor. In this way, the active 2D slice becomes a 2D gain/loss modulated material also exhibiting an index modulation on the wavelength scale. Our model considers an incident beam that propagates in plane, inside the active semiconductor slab, and along the largest diagonal of the rhombic structure. Integration is performed using paraxial approximation. Numerical results present evidence of filtering effects in a Gaussian beam with multiplicative white noise. The quantification of the beam improvement is estimated by means of the M^2 coefficient, which gives the relative distance between the evaluated profile and a perfect Gaussian beam. The M^2 value of the amplified beam approaches 1, meaning that all noise can be almost completely filtered out.

While systems containing gain and/or losses have previously almost never been considered, they have, however, been recently attracting a huge interest in the last years. Such unconventional systems have shown to hold novel unconventional properties such us symmetry breaking, unidirectional invisibility, cloaking, etc. and are finding feasible realizations and therefore experimental demonstrations precisely either in the field of optics and acoustics [Guo09, Rüt10, Fleu09, Zhu14]. Some of the such complex systems belong to the particular class of Parity-Time symmetric systems [Ben98], where the real and the imaginary modulations of the potential are de-phased by a quarter of the period of the modulation, but belong to the wider field of non-

Hermitian or complex potentials [Hor15, Ben15, Mir16] to which this thesis belongs.

In particular, complex optical crystals holding in-phase modulations of the gain and loss and index profile hold regimes of simultaneous non-diffractive propagation and non-diffusive beam broadening [Her14]. This result may represent a direct continuation of the results presented in [Kum12, Kum14 & Kum14]. Such self-collimation propagation, or dynamical localization, have more recently been demonstrated in complex 2D lattices with PT-symmetry [Bot15, Ahm17].

The work [Kum12] opened new perspectives in light manipulation on the micrometer scale for beams. Such effects described for continuous beams were later explored for the case of optical pulses in ref. [Loi12]; where the light beam shaping results in LMM form the basis of versatile and efficient technique for the formation of X-pulses in GLMM.

Also, some directly related works have been reported in acoustics, where 1D periodic LMM sonic crystals may be easily constructed by a layered alignment of lossy structures as refractive media. In such configuration, the frequency-selective spatial acoustic filtering effect was investigated [Ala16], showing that a sonic crystal flat lens can be used for narrow-band harmonic enhancement. There, the negative refraction acts on the spatial filtering of acoustic waves, analogously as in [Kum13]. Besides, an experimental confirmation of the high transmission bands predicted in ref. [Kum12] for LMM was reported in ref.[Ceb14], related to a decrease of the absorption around the Bragg frequencies for an array of porous layers embedded in air.

In parallel metallo-dielectric photonic crystals are nowadays being fabricated for a wide variety of applications, ranging from spatial diffraction management [Zha15], to energy harvesting and thermal emission modification [Ino13], therefore a deep understanding of their properties at optical frequencies stays relevant.

Finally, our initial ideas and investigations in the application of the beam management in BAS amplifiers started in conference proceedings [Her11, Her12, Her12-2] later lead to positive results either in amplifiers and in lasers [Her12-3, Rad13, Her14-2, Rad15]. In these cases the quality of the beam is improved while being amplified in edge emitting broad area semiconductor amplifiers with a periodic structuring of the electrical contacts, in both longitudinal

and lateral directions. Beyond these works it has also been demonstrated that two-dimensional periodic modulations of the pump profile (modulation both along and perpendicular to the optical axis) improve the emission from broad area semiconductor amplifiers by suppressing the modulation instability [Kuma14, Kuma16].

Therefore, periodical complex structures nowadays represent a fruitful playground for novel physical effects, with direct applications in the fields of optics and acoustics, in which I expect to have contributed by means of my PhD.

References

[Ada93] H. Adachihara, O. Hess, E. Abraham, P. Ru, and J. V. Moloney, *"Spatiotemporal chaos in broad-area semiconductor lasers"*, Journal of Optical Society of America B **10**, 658-665 (1993)

[Ala16] S. Alagoz, *"An analysis of the spatio-spectral acoustic filtering effect of sonic crystals"*, Chinese Journal of Physics 54, 788-794 (2016)

[Ahm17] W. W. Ahmed, R. Herrero, M. Botey, and K. Staliunas, *"Self-collimation in PT-symmetric crystals"*, To appear in Physical Review A

[Agr89] G. P. Agrawal and N. A. Olsson, *"Self-Phase modulation and spectral broadening of optical pulses in semiconductor laser amplifiers"*, Journal of Quantum Electronics 25, 2297 (1989)

[Bel06] P. A. Belov and Y. Hao, ***"****Subwavelength imaging at optical frequencies using a transmission device formed by a periodic layered metal–dielectric structure operating in the canalization regime****",*** Physical Review B **73**, 113110 (2006)

[Ben98] C. M. Bender, and S. Boettcher, *"Real spectra in non-Hermitian Hamiltonians having P-T symmetry"*, Physical Review Letters **80**, 5243 (1998)

[Ben07] C. M. Bender, *"Making sense of non-Hermitian Hamiltonians"*, Reports on Progress in Physics **70**, 947–1018 (2007)

[Bes66] V. I. Bespalov and V. I. Talanov, *"Filamentary Structure of Light Beams in Nonlinear Liquids"*, JETP Letters **3**, 307-309 (1966)

[Ber04] A. Berrier, M. Mulot, M. Swillo, M. Qiu, L. Thylén, A. Talneau, and S. Anand. *"Negative refraction at infrared wavelengths in a two-dimensional photonic crystal",* Physical Review Letters **93**, 073902 (2004)

[Bla00] A. Blanco, E. Chomski, S. Grabtchak, M. Ibisate, S. W. Leonard, C. Lopez, F. Meseguer, et al. (2000), "*Large-scale synthesis of a silicon photonic crystal with a complete three-dimensional bandgap near 1.5 micrometres*", Nature **405** (6785): 437–440 (2000)

[Bor80] see for instance M. Born and E. Wolf, *Principles of Optics*, Oxford: Perg-amon, 6th ed. (1980)

[Bot10] M. Botey, R. Herrero, and K. Staliunas. *"Light in materials with periodic gain-loss modulation on a wavelength scale"*, Physical Review A **82**, 013828 (2010)

[Bot11] M. Botey, R. Herrero, N. P. Kumar, R. Vilaseca, and K. Staliunas, *"Self-collimation and spatial filtering in 2D gain/loss periodic spatially modulated materials",* In European Quantum Electronics Conference (p. EI_P8). Optical Society of America (2011)

[Bot13] M. Botey, N. P. Kumar, R. Herrero, L. Maigyte, R. Pico, and K. Staliunas, *"Negative diffraction by a periodically modulated loss",* Transparent Optical Networks (ICTON), 15th International Conference on. IEEE, (2013)

[Bot13-2] M. Botey, Y. C. Cheng, V. Romero-Garcia, R. Picó, R. Herrero, V. Sánchez-Morcillo, K. Staliunas, "Unlocked evanescent waves in periodic structures", Optics Letters **38**, 1890-1892 (2013)

[Bot14] M. Botey, N. P. Kumar, L. Maigyte, R. Herrero, and K. Staliunas, *"Managing spatial diffraction through a periodic loss modulation",* In SPIE Photonics Europe (pp. 912710-912710). International Society for Optics and Photonics (2014)

[Bot15] M. Botey, M. Turduev, H. Kurt, R. Herrero and K. Staliunas, *"Self-collimation in 2D complex and PT-symmetric media"*, 17th International Conference on Transparent Optical Networks (ICTON), (2015)

[Bram97] M. Brambilla, L.A. Lugiato, F. Prati, L. Spinelli, W.J. Firth, Spatial soliton pixels in semiconductor devices, Phys. Rev. Lett. **79**, 2042 (1997)

[Buc09] J. Bucay, E. Roussel, J. O. Vasseur, P. A. Deymier, A. C. Hladky-Hennion, Y. Pennec, K. Muralidharan, B. Djafari-Rouhani, B. Dubus, *"Positive, negative, zero refraction, and beam splitting in a solid/air phononic crystal: theoretical and experimental study"*, Physical Review B **79,** 214305 (2009)

[Bur99] T. Burkhard, M. O. Ziegler, I. Fischer, and W. Elsäßer, *"Spatio-temporal dynamics of broad area semiconductor lasers and its characterization"*, Chaos Solitons & Fractals, **10**, 845–850 (1999)

[Ceb14] A. Cebrecos and R. Picó and V. Romero-García, A. M. Yasser, L. Maigyte, R. Herrero, M. Botey, V. J. Sánchez-Morcillo and K. Staliunas, *"Enhanced transmission band in periodic media with loss modulation"*, Applied Physics Letters **105**, 204104 (2014).

[Ceg08] D. de Ceglia, M. A. Vincenti, M. G. Cappeddu, M. Centini, N. Akozbek, A. D'Orazio, J. W. Haus, M. J. Bloemer, and M. Scalora, **"***Tailoring metallodielectric structures for superresolution and superguiding applications in the visible and near-IR ranges***",** Physical Review A **77**, 033848 (2008)

[Chen08] F. Chen, D. Gindre, and J. M. Nunzi, *"Tunable circularly polarized lasing emission in reflection distributed feedback dye lasers",* Optics Express **16,** 16746-16753 (2008)

[Chi03] D. Chigrin, S. Enoch, C. S. Torres, and G. Tayeb, **"***Self-guiding in two-dimensional photonic crystals***",** Optics Express **11**, 1203**–**1211 (2003)

[Cic11] A. Cicek, O. A. Kaya, B.J. Bulug, *"Wide-band all-angle acoustic self-collimation by rectangular sonic crystals with elliptical bases"*, Journal of Physics D: Applied Physics **44,** 205104 (2011)

[Coh98] C. Cohen-Tannoudji, J. Dupont-Roc, G. Grynberg, *"Atom Photon Interactions: Basic Processes and Applications"*, John Wiley & Sons, New York (1998)

[Cou28] Richard Courant; Kurt Otto Friedrichs; Hans Lewy *"Über die partiellen Differenzengleichungen der mathematischen Physik*". Mathematische Annalen **100,** 32–74 (1928)

[Col10] E. Colak, A. O. Cakmak, A. E. Serebryannikov, and E. Ozbay, **"***Spatial filtering using dielectric photonic crystals at beam-type excitation***",** Journal of Applied Physics **108**, 113106 (2010)

[Cre14] D. Creeden, B. R. Johnson, S. D. Setzler and E. P. Chicklis, *"Resonantly pumped Tm-doped ber laser with > 90% slope efficiency"*, Optics Letters **39**, 470 - 473 (2014)

[Crys] CrystalWave software by Photon Design Ltd., http://www.photond.com.

[Cub03] E. Cubukcu, K. Aydin, E. Ozbay, S. Foteinopoulou, and C. M. Soukoulis. *"Electromagnetic waves: Negative refraction by photonic crystals"*, Nature **423**, 604 (2003)

[Dre74] K. H. Drexhage, *"Interaction of Light with monomolecular dye layers"*, in: E. Wolf (Ed.), Progress in Optics, vol. 12, North- Holland Publishing Co, Amsterdam, pp. 163–232 (1974)

[Dud06] J. M. Dudley, G. Genty, and S. Coen, *"Supercontinuum generation in photonic crystal fiber"*, Reviews of Modern Physics **78** (4), 1135 (2006)

[Esp07] Víctor Espinosa, Víctor J. Sánchez-Morcillo, Kestutis Staliunas, Isabel Pérez-Arjona, and Javier Redondo, *"Subdiffractive propagation of ultrasound in sonic crystals"*, Physical Review B **76**, 140302 (2007)

[Fang05] N. Fang, H. Lee, C. Sun, and X. Zhang, ***"Subdiffraction limited optical imaging with a silver superlens"*,** Science **308**, 534**–**537 (2005)

[Fleu15] R. Fleury, F. Monticone, and A. Alù, *"Invisibility and cloaking: Origins, present, and future perspectives",* Physical Review Applied **4**, 037001 (2015)

[Fri15] H. Fritsche, F. Ferrario, R. Koch, B. Kruschke, U. Pahl, S. Pueger, A. Grohe, W. Gries, F. Eibl, S. Kohl, M. Dobler, *"Direct diode lasers and their advantages for materials processing and other applications"*, Proceedings of SPIE, Laser Joining II, 9356, 93560I-1-93560I-6 (2015)

[Gol88] L. Goldberg and M.K. Chun, *"Injection locking characteristics of a 1 W broad stripe laser diode"*, Applied Physics Letters **53**, 1900-1902 (1988)

[Guo09] A. Guo, G. J. Salamo, D. Duchesne, R. Morandotti, M. Volatier-Ravat, V. Aimez, and D. N. Christodoulides, *"Observation of P T-symmetry breaking in complex optical potentials.",* Physical Review Letters **103**, 093902 (2009)

[Her11]R. Herrero, M. Botey, N. Kumar, K. Staliunas, "Dispersion management in spatially modulated broad band semiconductors", 13th International Conference on Transparent Optical Networks (ICTON), Institute of Electrical and Electronics Engineers (IEEE) (2011)

[Her12] R. Herrero, M. Botey, N. Kumar and K. Staliunas, *"Spatial noise reduction in broad area semiconductors"*, 2012 14th International Conference on Transparent Optical Networks (ICTON), Institute of Electrical and Electronics Engineers (IEEE) (2012)

[Her12-2] R. Herrero, M. Botey, N. P. Kumar, and K. Staliunas, *"Improving beam quality in broad area semiconductor amplifiers",* SPIE Photonics Europe. International Society for Optics and Photonics (2012)

[Her12-3] R. Herrero, M. Botey, M. Radziunas, and K. Staliunas, *"Beam shaping in spatially modulated broad-area semiconductor amplifiers"*, Optics letters **37**, 5253-5255 (2012)

[Her14] R. Herrero, M. Botey, and K. Staliunas, *"Nondiffractive-nondiffusive beams in complex crystals"*, Physical Review A **89**, 063811 (2014)

[Her14-2] R. Herrero, S. Kumar, M. Radziunas, M. Botey, and K. Staliunas, *"Improving beam quality in broad area semiconductor amplifiers"*, 16th International Conference on Transparent Optical Networks (ICTON), Institute of Electrical and Electronics Engineers (IEEE) (2014)

[Ho90] K. M. Ho, C. T. Chan, and C. M. Soukoulis, "*Existence of a photonic gap in periodic dielectric structures*", Physical Review Letters **65**, 3152-3155 (1990)

[Hor15] S. A. R. Horsley, M. Artoni, and G. C. La Rocca, *"Spatial Kramers-Kronig relations and the reflection of waves",* Nature Photonics **9**, 436–439 (2015)

[Hsue09] Y. C. Hsue and T. J. Yang, "Applying a modified plane-wave expansion method to the calculations of transmittivity and reflectivity of a semi-infinite photonic crystal", Phys. Rev. E **70**, 016706 (2004)

[Ill04] R. Illiewa, C. Etrich, U. Peschel, and F. Lederer M. Augustin, H.-J. Fuchs, D. Schelle, E.-B. Kley, S. Nolte, and A. Tünnermann, *"Diffractionless propagation of light in a low index photonic-crystal film"*, Applied Physics Letters **85**, 5854 (2004)

[Ino13] K. Inoue, and K. Ohtaka, (Eds.), "*Photonic crystals: physics, fabrication and applications",* (Vol. 94). Springer series in Optical Sciences (2013)

[ISO05] ISO Standard 11146, ISO Standard 11146*, "Lasers and laser-related equipment. Test methods for laser beam widths, divergence angles and beam propagation ratios"* (2005)

[Jia11] L. Jia and E. L. Thomas, *"Two-pattern compound photonic crystals with a large complete photonic band gap",* Physical Review A **84**, 033810 (2011)

[Jia11a] L. Jia and E. L. Thomas, *"Theoretical study on photonic devices based on a commensurate two-pattern photonic crystal"*, Optics Letters **36**, 3416–3418 (2011)

[Joa11] J. D. Joannopoulos et al. "*Photonic crystals: molding the flow of light"*, Princeton university press (2011)

[Joh87] S. John. *"Strong localization of photons in certain disordered dielectric superlattices"*, Physical Review Letters **58**, 2486 (1987)

[Joh01] S. G. Johnson and J. D. Joannopoulos, "*Block-iterative frequency-domain methods for Maxwell's equations in aplane wave basis "*, Optics Express **8**, 173–180 (2001)

[Joy82] W. B. Joyce, "Carrier transport in double-heterostructure active layers", Journal of Applied Physics **53,** 7235 (1982)

[Kal08] M. A. Kaliteevski, S. Brand, J. Garvie-Cook, R. A. Abram, and J. M. Chamberlain. *"Terahertz filter based on refractive properties of metallic photonic crystal",* Optics Express **16**, 7330 (2008)

[Kos99] H. Kosaka, T. Kawashima, A. Tomita, M. Notomi, T. Tamamura, T. Sato, and S. Kawakami, *"Self-collimating phenomena in photonic crystals"*, Applied Physics Letters **74**, 1212-1214 (1999)

[Kum11] R. Herrero, M. Botey, N. Kumar, K. Staliunas, "Dispersion management in spatially modulated broad band semiconductors", 13th International Conference on Transparent Optical Networks. Institute of Electrical and Electronics Engineers (IEEE), (2011)

[Kum12] N. Kumar, M. Botey, R. Herrero, and K. Staliunas *"High-directional wave propagation in periodic loss modulated materials"*, Photonics and Nanostructures-Fundamentals and Applications **10.4**, 644-650 (2012)

[Kum13] N. Kumar, M- Botey, R. Herrero and K. Staliunas, *"Flat lensing by periodic loss-modulated materials"*, Journal of the Optical Society of America B **30.10**, 2684-2688 (2013)

[Kum14] N. Kumar, L. Maigyte, M. Botey, R. Herrero, and K. Staliunas, *"Beam shaping in two-dimensional metallic photonic crystals"*, Journal of the Optical Society of America B **31.4** 686-690 (2014)

[Kuma14] S. Kumar, R. Herrero, M. Botey, and K. Staliunas, *"Suppression of modulation instability in broad area semiconductor amplifiers",* Optics letters **39**, 5598-5601 (2014)

[Kuma16] S. Kumar, W. W. Ahmed, R. Herrero, M. Botey, M. Radziunas, and K. Staliunas, *"Stabilization of Broad Area Semiconductor Amplifiers by Spatially Modulated Potentials"*, Nonlinear Dynamics: Materials, Theory and Experiments, pp. 139-151) Springer International Publishing (2016)

[Kru99] Krupke W. F.: *"Advanced diode-pumped solid state lasers (DPSSLs): near-term trends and future prospects"*, *Proceedings of SPIE*, High-Power Laser Ablation II, 3885, 21 - 32 (1999)

[Lan91] Lang, Robert J; Larsson, Anders G; Cody, Jeffrey G, *"Lateral modes of broad area semiconductor lasers: Theory and experiment"*, IEEE Journal of Quantum Electronics **27**,3, 312-320 (1991)

[Lau09] V. Laude, Y. Achaoui, S. Benchabane, and A. Khelif, "Evanescent Bloch waves and the complex band structure of phononic crystals", Phys. Rev. B **80**, 092301 (2009)

[Lee05] H. Lee, Y. Xiong, N. Fang, W. Srituravanich, S. Durant, M. Ambati, C. Sun, and X. Zhang, ***"****Realization of optical superlens imaging below the diffraction limit****",*** New Journal of Physics **7**, 255 (2005)

[Lit09] N.M. Litchinitser, V.M. Shalaev, *"Metamaterials: transforming theory into reality"*, Journal of Optical Society of America, B **26**, B161-B169 (2009)

[Loi12] Yu. Loiko, M. Botey, R. Herrero, K. Staliunas, *"Formation of Xpulses in gain/loss modulated materials"*, Optics Express **20**, 11271–11276 (2012)

[Lon09] S. Longhi, *"Bloch oscillations in complex crystals with PT symmetry"*, Physical Review Letters **103**, 123601 (2009)

[Lon10] S. Longhi, *"Spectral singularities and Bragg scattering in complex crystals"*, Physical Review A **81**, 022102 (2010)

[Luc05] V. Lucarini, K. Peiponen, J. Saarinen and E. M. Vartiainen, *"Kramer Kronig relation in Optical Material research"*, Springer series in Optical Sciences. ISBN: 978-3-540-23673-3 (2005)

[Luo02] C. Luo, S. G. Johnson, J. D. Joannopoulos, and J. B. Pendry, *"All-angle negative refraction without negative effective index"*, Physical Review B **65**, 201104 (2002)

[Mak08] K. G. Makris, R. El-Ganainy, D. N. Christodoulides, and Z. H. Musslimani, *"Beam dynamics in PT-symmetric optical lattices"*, Physical Review Letters **100**, 103904 (2008)

[Mai10] L. Maigyte, T. Gertus, M. Peckus, J. Trull, C. Cojocaru, V. Sirutkaitis, and K. Staliunas, *"Signatures of light-beam spatial filtering in a three-dimensional photonic crystal"*, Physical Review A **82**, 043819 (2010)

[Mai13] L. Maigyte, V. Purlys, J. Trull, M. Peckus, C. Cojocaru, D. Gailevicius, M. Malinauskas, and K. Staliunas, *"Flat lensing in the visible frequency range by woodpile photonic crystals",* Optics Letters **38**, 2376–2378 (2013)

[Mai15] L. Maigyte and K. Staliunas, *"Spatial filtering with photonic crystals"*, Applied Physics Reviews **2**, 011102 (2015).

[Man03] S. K. Mandre, I. Fischer and W. Elsässer, *"Control of the spatiotemporal emission of a broad-area semiconductor laser by spatially filtered feedback"*, Optics Letters **28**, 1135-1137 (2003)

[Mart90] J. Martorell, and N. M. Lawandy. *"Observation of inhibited spontaneous emission in a periodic dielectric structure"*, Physical Review Letters **65,** 1877 (1990)

[Mir16] M. A. Miri, and A. Alù, *"Nonlinearity-induced PT-symmetry without material gain"*, New Journal of Physics **18**, 065001 (2016)

[Nis08] Y. Nishijima, K. Ueno, S. Juodkazis, V. Mizeikis, H. Misawa, M. Maeda, and M. Minaki, *"Tunable single-mode photonic lasing from zirconia inverse opal photonic crystals"*, Optics Express **16**, 13676–13684 (2008)

[Naj15] S. P. Najda, P. Perlin, T. Suski, L. Marona, M. Boćkowski, M. Leszczyński, P. Wiśniewski, R. Czernecki, R. Kucharski, G. Targowski, S. Watson, A. E. Kelly, M. A. Watson, P. Blanchard, H. White, *"AlGaInN laser diode technology for free-space telecom applications"*, *Proceedings of SPIE*, Laser Transmitters, 9354, 93540Q-1-93540Q-11 (2015)

[Noda03] Y. Akahane, T, Asano, B. S. Song, and S. Noda, *"High-Q photonic nanocavity in a two-dimensional photonic crystal"*, Nature, **425**, 944-947 (2003)

[Oul07] R. Oulton, B.D. Jones, S. Lam, A.R.A. Chalcraft, D. Szymanski, D. O'Brien, T.F. Krauss, D. Sanvitto, A.M. Fox, D.M. Whittaker, M. Hopkinson, and M.S. Skolnick *"Polarized quantum dot emission from photonic crystal nanocavities studied under moderesonant enhanced excitation"*, Optics Express **15** 17221–17230 (2007)

[Par03]P. V. Parimi, W. T. Lu, P. Vodo, and S. Sridhar, *"Imaging by flat*

lens using negative refraction", Nature **426**, 404 (2003)

[Pen00] J. B. Pendry. *"Negative refraction makes a perfect lens"*, Physical Review Letters **85**, 3966 (2000)

[Pen06] J. Pendry, *"Metamaterials – An Overview, Photonic Metamaterials: From Random to Periodic"*, Technical Digest, Optical Society of America (2006)

[Pér07] Is. Pérez-Arjona, V.J. Sánchez-Morcillo, J. Redondo, V. Espinosa, and K. Staliunas, *"Theoretical prediction of the nondiffractive propagation of sonic waves through periodic acoustic media"*, Phyical Review B **75**, 014304 (2007)

[Pra04] W. Prather, S. Shi, M. Pustai, C. Chen, S. Venkataraman, A. Sharkawy, J. Schneider, and J. Murakowski, *"Dispersion-based optical routing in photonic crystals"*, Optics Letters **29**, 50-52 (2004)

[Raa02] V. Raab, and R. Menzel, *"External resonator design for high-power laser diodes that yields 400mW of TEM00 power"*, Optics Letters **27**, 167-169 (2002)

[Rad11] M. Radziunas and K. Staliunas, *"Spatial "rocking" in broad-area semiconductor lasers"*, Europhysics Letters **95**, 14002 (2011)

[Rad13] M. Radziunas, M. Botey, R. Herrero, and K. Staliunas, *"Intrinsic beam shaping mechanism in spatially modulated broad area semiconductor amplifiers"*, Applied Physics Letters **103**, 132101-132101-4 (2013)

[Rad15] M. Radziunas, R. Herrero, M. Botey, and K. Staliunas, *"Far-field narrowing in spatially modulated broad-area edge-emitting semiconductor amplifiers"*, Journal of Optical Society of America **32**, 993-1000 (2015)

[Ram03] S. A. Ramakrishna, and J. B. Pendry, *"Removal of absorption and increase in resolution in a near-field lens via optical gain",* Physical Review B **67**, 201101 (2003)

[Ray88] J. W. S. Rayleigh, *"On the remarkable phenomenon of crystalline reflexion described by Prof. Stokes"*, Philosophical Magazine **26**, 256–265 (1888)

[Russ03] P. Russell, *"Photonic crystal fibers"*, Science, **299** (5605), 358-362 (2003)

[Rom10] V. Romero-García, J. V. Sánchez-Pérez, S. Castiñeira-Ibáñez, and L. M. Garcia-Raffi, *"Evidences of evanescent Bloch waves in phononic crystals"*, Applied Physics Letters **96**, 124102 (2010).

[Rüt10] C. E. Rüter, K. G. Makris, K, R. El-Ganainy, D. N. Christodoulides, M. Segev, and D. Kip, *"Observation of parity–time symmetry in optics"*, Nature physics **6**, 192-195 (2010)

[Sak04] K. Sakoda, *"Optical properties of photonic crystals"*, Vol. 80. Springer Science & Business Media (2004)

[Sav09] S. Savo, E. Gennaro, and A. Andreone, *"Superlensing properties of one-dimensional dielectric photonic crystals*", Optics Express **17**, 19848-19856 (2009)

[Scu01] M.O. Scully, and M.S. Zubairy, *"Quantum Optics"*, Cambridge University Press (2001)

[Ser06] J. Serbin, and M. Gu, *"Experimental evidence for superprism effects in three-dimensional polymer photonic crystals"*, Advanced Materials **18**, 221 (2006)

[Shel01] R. A. Shelby, D. R. Smith, and S. Schultz, *"Experimental verification of a negative index of refraction"*, Science **292**, 77-79. (2001).

[Shi08] J. J. Shi, S. C. S. Lin, and T. S. Huang, *"Wide-band acoustic collimating by phononic crystal composites"*, Applied Physics Letters **92,** 111901 (2008)

[Sou93] C. M. Soukoulis (Ed.), *"Photonic Band Gaps and Localization, Series B: Physics"*, Vol. **308**, NATO Advanced Studies Institute, New York (1993)

[Souk12] C. M. Soukoulis ed. "*Photonic crystals and light localization in the 21st century"*. Vol. **563**. Springer Science & Business Media, (2012)

[Sta06] K. Staliunas and R. Herrero, *"Nondiffractive propagation of light in photonic crystals"*, Physical Review E **73**, 016601 (2006)

[Sta06a] K. Staliunas, *"Subdiffractive solitons of Bose–Einstein condensates in time-dependent optical lattices"*, Physical Review E **73**, 065603 (2006)

[Sta09] K. Staliunas, R. Herrero, and R. Vilaseca, *"Subdiffraction and spatial filtering due to periodic spatial modulation of the gain-loss profile"*, Physical Review A **80**, 013821 (2009)

[Sta09a] K. Staliunas, and V. J. Sa´nchez-Morcillo, *"Spatial filtering of light by chirped photonic crystals"*, Physical Review A **79**, 053807 (2009)

[Swi11] G. P. Swift, A. J. Gallant, N. Kaliteevskaya, M. A. Kaliteevski, S. Brand, D. Dai, A. J. Baragwanath, I. Iorsh, R. A. Abram, and J. M. Chamberlain, *"Negative refraction and the spectral filtering of terahertz radiation by a photonic crystal prism",* Optics Letters **36**, 1641 (2011)

[Taf00] A. Taflove, and S.C. Hagness, *"Computational Electro-Dynamics: The Finite Difference Time Domain Method, 2nd ed."*, Artech House, Norwood, MA (2000)

[Taf80] A. Taflove *"Application of the finite-difference time-domain method to sinusoidal steady state electromagnetic penetration problems"* IEEE Transactions on Electromagnetic Compatibility. 22 (3) (1980)

[Tia11] J. Tiana, J. Zamora, C. Nistor, V. Roppo, L. Maigyte, A. Aragoneses; N. Kumar, C. Martinez, J. Fernandez, C. Serrat, J.L. Font, R. Herrero, C. Cojocaru, J. Trull, C. Masoller, K. Staliunas, M.C. Torrent, J. Garcia, R. Vilaseca, "*Research activities of the group on nonlinear dynamics, nonlinear optics and lasers (DONLL) at the Universitat Politècnica de Catalunya" (Campus de Terrassa),* Óptica Pura y Aplicada **44**, (2011) (2011)

[Tru11] J. Trull, L. Maigyte, V. Mizeikis, M. Malinauskas, S. Juodkazis, C. Cojocaru, M. Rutkauskas, M. Peckus, V. Sirutkaitis, and K. Staliunas,

"*Formation of collimated beams behind the woodpile photonic crystal*", Physical Review A **84**, 033812 (2011)

[Tur15] M. Turduev, I.H. Giden, and H. Kurt, *"Design of flat lens-like graded index medium by photonic crystals: Exploring both low and high frequency regimes"*, Optics Communications **339**, 22 (2015).

[Ult03] E. A. Ultanir, D. Michaelis, F. Lederer, and G. I. Stegeman, *"Stable spatial solitons in semiconductor optical amplifiers"*, Optics Letters **28**, 251–253 (2003)

[Ult06] E. A. Ultanir, D. N. Christodoulides, and G. I. Stegeman, *"Spatial modulation instability in periodically patterned semiconductor optical amplifiers"*, Journal of the Optical Society of America B **23**, 341-346 (2006)

[Van08] O. Vanbésien, N. Fabre, X. Mélique, and D. Lippens, *"Photonic-crystal-based cloaking device at optical wavelengths",* Applied Optics **47**, 1358-1362 (2008)

[Ves68] V. G. Veselago, *"The electrodynamics of substances with simultaneously negative values of ε and μ"*, Soviet Physics Uspekhi **10**, 509 (1968)

[Vin09] M. A. Vincenti, D. de Ceglia, V. Rondinone, A. Ladisa, A. D'Orazio, M. J. Bloemer, and M. Scalora, ***"****Loss compensation in metal–dielectric structures in negative-refraction and super-resolving regimes****",*** Physical Review A **80**, 053807 (2009)

[Vla05] Yurii A. Vlasov, Martin O'Boyle, Hendrik F. Hamann, and Sharee J. McNab, *"Active control of slow light on a chip with photonic crystal waveguides"*, Nature **438**, 7064 65-69 (2005)

[Vuk03] P. Vukusic, and J. R. Sambles, *"Photonic structures in biology*", Nature, **424**, 6950, 852-855 (2003)

[Wan04] X. Wang, Z. F. Ren, and K. Kempa, *"Unrestricted superlensing in a triangular two dimensional photonic crystal"*, Optics Express 12, 2919–2924 (2004)

[Wu06] Q. Wu, E. Schonbrun, and W. Park, *"Tunable superlensing by a mechanically controlled photonic crystal"*, Journal Optical Society of America B **23,** 479-484 (2006)

[Xu13] T. Xu, A. Agrawal, M. Abashin, K. J. Chau, and H. J. Lezec, *"All-angle negative refraction and active flat lensing of ultraviolet light"*, Nature **497**, 470-474 (2013).

[Yee66] K. Yee *"Numerical solution of initial boundary value problems involving Maxwell's equations in isotropic media*". IEEE Transactions on Antennas and Propagation. 14 (3): 302–307 (1966)

[Yab87] E. Yablonovitch, *"Inhibited spontaneous emission in solid-state physics and electronics"*, Physical Review Letters **58**, 2059 (1987)

[Zen87] R. Zengerle, *"Light propagation in singly and doubly periodic planar waveguides"*, Journal of Modern Optics **34**, 1589 (1987)

[Zha15] L. Zhang, L. Chen, Z. Zhang, W. Wang, Y. Zhao, K. Song, and C. Kang, *"Extraordinary refraction and self-collimation properties of multilayer metallic-dielectric stratified structures"*, Physica B: Condensed Matter **457**, 269 (2015)

[Zhu14] X. Zhu, H. Ramezani, C. Shi, J. Zhu, and X. Zhang, "*PT-Symmetric Acoustics"*, Physical Review X **4**, 031042 (2014)